



Cite this: *Chem. Sci.*, 2025, **16**, 4971

## Metal ferrite derivative chemical looping systems: a review towards a multiscale approach for technology readiness enabling clean energy conversion and carbon neutrality

Tanay A. Jawdekar, † Ishani Karki Kudva, † Sudeshna Gun, Shekhar G. Shinde, Ashin A. Sunny, Zhuo Cheng and Liang-Shih Fan \*

Chemical looping technologies offer a promising pathway for clean energy production, addressing the urgent need for decarbonization in light of escalating global energy demands and climate change concerns. This review explores the metal ferrite oxygen carriers in chemical looping applications, emphasizing their versatility in handling diverse feedstocks—from gases like methane to solids like plastics—and their robust performance in terms of stability and efficiency. The ferrite derivative chemical looping reactions involve the transfer of lattice oxygen from the metal ferrites to the fuel, enhancing fuel conversion without direct emission of pollutants. The structural and functional advantages of ferrites, including their ability to regenerate and sustain repeated redox cycles, are highlighted. Innovations in ferrite-based chemical looping, from small-scale laboratory setups to pilot-scale installations, demonstrate significant advancements in achieving high energy–exergy efficiencies with minimal ecological impact. The review also identifies ongoing challenges, such as the stability and effectiveness of metal ferrite oxygen carriers, suggesting improvements through material engineering and process optimization. This work aims to deepen understanding of ferrite oxygen carriers and propel forward their application in scalable, commercially viable clean energy solutions.

Received 31st August 2024  
Accepted 25th February 2025

DOI: 10.1039/d4sc05865h  
[rsc.li/chemical-science](http://rsc.li/chemical-science)

### 1 Introduction

The unprecedented increase in energy demand coupled with a growing concern for climate change has created an impetus for clean energy production.<sup>1</sup> Although a great emphasis is observed on harnessing energy from renewable sources, the U.S. Energy Information Administration has projected that more than 50% of the world's energy demand will be dependent upon fossil-based energy sources by 2050.<sup>2</sup> The growing industrial sector consumes ~33% of the total energy produced in the U.S., which amounts to nearly 26.7 quadrillion British thermal units (BTU).<sup>3</sup> The production of commodity chemicals like syngas, hydrogen (H<sub>2</sub>), methanol (CH<sub>3</sub>OH), ethanol (C<sub>2</sub>H<sub>5</sub>OH), ammonia (NH<sub>3</sub>), etc., via state-of-the-art technologies like auto-thermal reforming (ATR), steam methane reforming (SMR), Haber–Bosch process, etc. consumes ~35% of total industrial energy.<sup>4</sup> Although these technologies have been established for decades and have proven to be economical at larger scales of operation, they are challenged by carbon deposition and poor catalyst stability, leading to the formation of

undesirable side products.<sup>1</sup> This results in huge capital investment and high operating costs to comply with environmental protection policies. International treaties like the Paris Agreement aim to limit atmospheric CO<sub>2</sub> concentration below 430 ppm by 2030, necessitating the de-carbonization of industrial processes.<sup>5,6</sup>

Chemical looping (CL) is an emerging versatile alternative to produce commodity chemicals with inherent emission control.<sup>7–10</sup> This technology involves splitting the reaction scheme into a series of steps, facilitating complete fuel conversion, inherent product separation, and higher energy–exergy efficiencies.<sup>11–15</sup> Splitting of the reaction scheme is facilitated by a metal oxide carrier circulating within interconnected reactors and undergoing subsequent reduction and regeneration cycles.<sup>16,17</sup> During the reduction reaction, the metal oxide carrier donates its lattice oxygen to the fuel, resulting in the complete conversion of the fuel to the desired products (carbon dioxide – CO<sub>2</sub>, steam – H<sub>2</sub>O, or carbon monoxide – CO, H<sub>2</sub>). This lattice oxygen is then replenished using oxidizing gases like air, steam, or CO<sub>2</sub>, thus completing the redox loop. The overall reaction scheme remains the same as combustion or reforming.<sup>18,19</sup>

Breaking down the reaction scheme in this manner enables the isolation of the pure products without the need for

William G. Lowrie Department of Chemical and Biomolecular Engineering, The Ohio State University, Columbus, OH 43210, USA. E-mail: fan.1@osu.edu

† These authors have contributed equally to this work and are co-first authors.



a separation unit after the reactor.<sup>20</sup> While breaking the reaction into several steps helps to optimize each individual step to obtain near thermodynamic yields, the absence of direct contact of fuel and oxidizing gases at high temperatures mitigates the formation of pollutants like dioxins and nitrous oxides ( $\text{NO}_x$ ).<sup>21–23</sup> The high-grade heat produced during the regeneration step can cater to the low-grade heat requirement in the reducer reactor, thus eliminating any external heat requirement.<sup>23</sup> Moreover, advancements in efficient heating solutions offering near-unity conversion of renewable energy to heat negate the possible hindrance to the implementation of CL technologies requiring additional thermal input.<sup>24</sup>

The choice of the metal oxide carrier plays a pivotal role in determining the technical feasibility and the economic viability of this technology.<sup>5,25</sup> Transition metal oxides are highly favored for the CL process due to the high number of valence shell

electrons, which facilitate ionic diffusion, providing a large number of active sites and correspondingly high reactivity.<sup>26</sup> Several transition metal oxides, including but not limited to nickel oxide ( $\text{NiO}$ ), copper oxide ( $\text{CuO}$ ), iron oxide ( $\text{Fe}_2\text{O}_3$ ), chromium oxide ( $\text{Cr}_2\text{O}_3$ ), vanadium oxide ( $\text{V}_2\text{O}_5$ ), manganese oxide ( $\text{Mn}_2\text{O}_3$ ), cobalt oxide ( $\text{Co}_3\text{O}_4$ ), ceria ( $\text{CeO}_2$ ), etc., have been tested as probable candidates for the different CL schemes.<sup>27–35</sup> Iron-based oxygen carriers (OC) have garnered increased attention due to their favorable thermodynamics towards many CL applications, environmentally friendly nature, abundance, and low cost.<sup>28</sup> However, iron oxide faces several drawbacks, such as poor cyclic stability, poor kinetics, and high sintering.<sup>30,36,37</sup> In order to eliminate the challenges associated with iron oxide carriers, additional active metal oxides, dopants, promoters, binders, and inert supports are incorporated, creating a class of OC that can be classified as ferrite-based

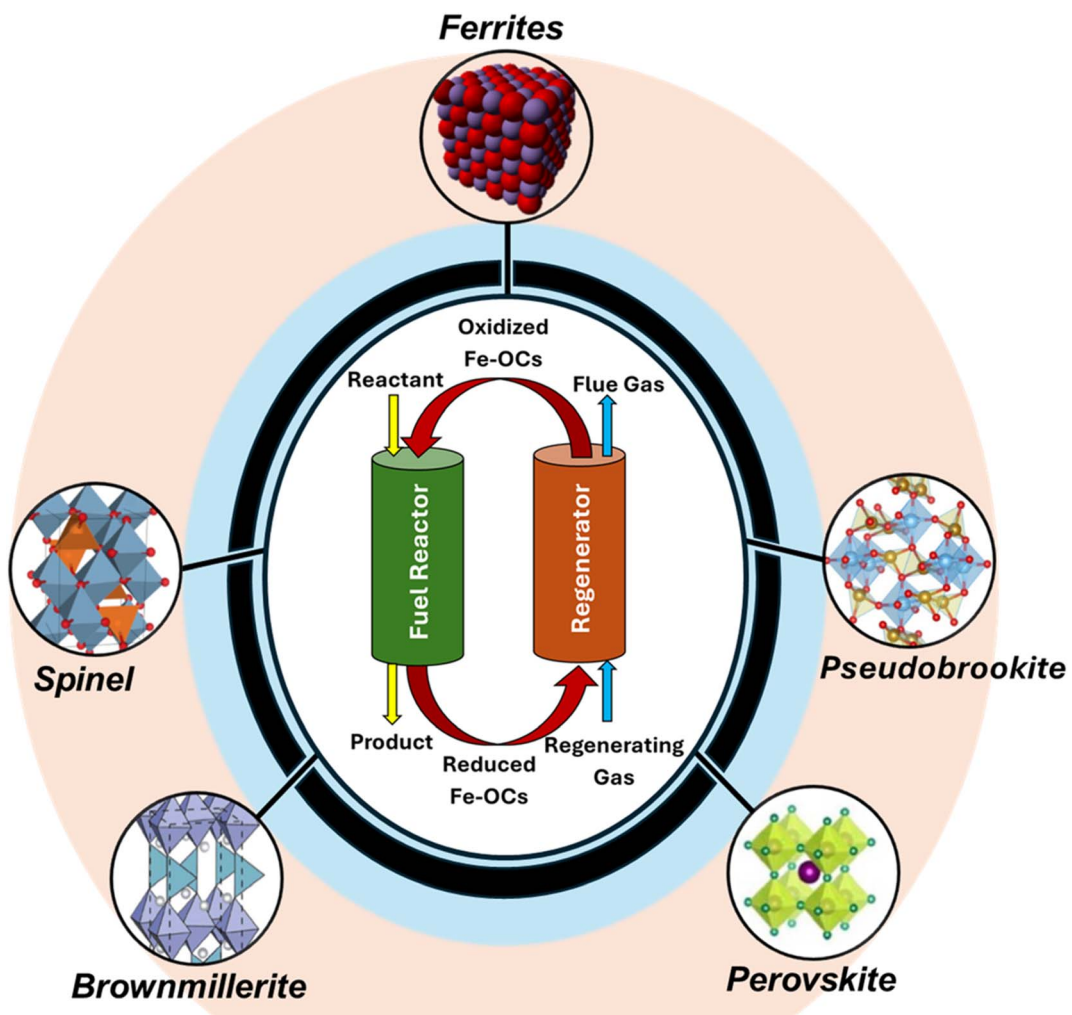


**Fig. 1** Prominence of metal ferrite derivatives in chemical looping. Brownmillerite structure adapted with permission from ref. 39. Copyright 2009 Springer Nature. Pseudobrookite structure adapted with permission from ref. 40. Copyright 2023 Elsevier. Perovskite structure adapted from a 2022 article published by MDPI (ref. 41) under a Creative Commons (CC BY) License. Spinel structure adapted from a 2020 article published by Springer Nature (ref. 42) under a Creative Commons Attribution 4.0 International (CC BY 4.0) License.



oxygen carriers (Fe-OC).<sup>38</sup> As illustrated in Fig. 1, the development of various Fe-OC composites with different crystal structures like spinel, brownmillerite, perovskite, and pseudobrookite has been of central importance to various CL applications.

Fe-OCs have demonstrated thermodynamic superiority, capacity to handle versatile feedstocks ranging from gases like methane ( $\text{CH}_4$ ) to solids like waste plastics, stable cyclic performance for an extended period of operation, and have proven to be suitable for several CL applications, including chemical looping combustion (CLC), gasification (CLG), partial oxidation (CLPO), reforming (CLR), and hydrogen generation (CLHG).<sup>43–54</sup> The commercialization potential of the CL technology has been realized through successful demonstrations at bench-scale, sub-pilot scale, and pilot-scale testing using Fe-OCs. These developments highlight the multiscale approach for implementing Fe-OC for multiphase reaction engineering.<sup>55</sup> While the superiority of Fe-OC has been established for a long time, a comprehensive review for understanding the role of each component incorporated in various ferrites is missing in the literature. This insight is crucial to achieving harmony between the chemical and physical properties of the OC and fine-tuning the OC composition for specific commercial applications. This review aims to understand the influence of different components on thermodynamics, the underlying mechanisms, the overall performance of ferrite OCs, and the feasibility of specific CL applications. This knowledge would be critical in tailoring and optimizing the OC composition, which is essential for the economic viability of the commercial process.

## 2 Fundamental insights into Fe-OC for performance enhancement

Understanding the fundamentals of ferrites as versatile OC is vital for their applications in CL systems. This section provides an in-depth exploration of the key fundamental aspects of Fe-OCs, focusing on how ionic diffusion influences its morphology, volume expansion, and structural integrity. It also examines the role of oxygen vacancies in enhancing lattice oxygen transport and overall reactivity. Additionally, the formation of core-shell structures and their advantages for improving stability and preventing sintering are discussed.

### 2.1. Role of ionic diffusion in Fe-OC

The morphology of Fe-OC is pivotal in influencing its surface area, reaction kinetics, and structural integrity, thereby directly affecting its overall performance. It is closely tied to ionic diffusion and changes in molar volume. The ionic diffusion during Fe-OC oxidation results in a net outward transport of Fe ions from the core to the surface, where they are oxidized to form  $\text{Fe}_2\text{O}_3$ . This results in an inward progressing  $\text{Fe}_2\text{O}_3$  layer, leading to the complete oxidation of Fe-OC particle. Simultaneously, the oxidation reaction leads to volume expansion of Fe-OC, as observed from macroscopic studies on Fe-Ti OC by Li *et al.* and microscopic investigations on  $\text{Fe}_2\text{O}_3$  OC by Cheng

*et al.*<sup>56,57</sup> The volume increases from 31.7 to 54.4  $\text{cm}^3 \text{ mol}^{-1}$  in the case of  $\text{FeTiO}_3$  converting to  $\text{Fe}_2\text{TiO}_5$  and from 7.1 to 30.5  $\text{cm}^3 \text{ mol}^{-1}$  in the case of Fe converting to  $\text{Fe}_2\text{O}_3$ , both of which exhibit larger volume changes compared to many other transition metal oxides like NiO and CuO investigated in the literature.<sup>57</sup> The high molar volumes of Fe-OC enhance the transport of Fe ions from the core to the surface and provide greater surface area for redox reactions, making Fe-OCs an attractive choice for CL applications.<sup>58</sup> Therefore, understanding these ionic diffusion processes and the resulting changes in molar volume is essential for predicting and controlling the morphological transformations that occur during the reduction and oxidation cycles of Fe-OCs.

The performance and macroscopic behavior of metal oxides are heavily influenced by their nanoscale morphology, which is shaped by solid-state ionic diffusion. This morphology can vary significantly from single-metal systems to bimetallic ones. Lang *et al.* discuss the evolution of nanoscale morphology in such contexts. During the oxidation of Fe particles, the growth of nanostructures, such as nanowires and nanopores, depends significantly on the surface curvature of the grains. This process is governed by a stress-driven mass transport mechanism, where the curvature of  $\text{Fe}_2\text{O}_3$  grains determines the type of nanostructure that forms. Positive surface curvature leads to the outward diffusion of Fe atoms, resulting in perpendicular nanowire growth, while negative surface curvature promotes oxide growth, leading to the formation of nanopores within the grain, as shown in Fig. 2(a) and (b), respectively.<sup>58</sup> Lang *et al.* further extended the scope of their research to include bimetallic Fe-Ti particles. The difference in the diffusion rate of Fe ions compared to Ti ions resulted in the formation of nanobelts on the surface. Repeated redox cycles make these structures highly porous with improved morphological stability, as depicted in Fig. 2(c).<sup>59</sup> These studies highlight the critical role of ionic diffusion in the design and performance of Fe-OCs.

### 2.2. Effect of oxygen vacancy in Fe-OCs

During the reduction step of CL applications, the lattice oxygen from the Fe-OC, whether from the surface or bulk, is transferred to the hydrocarbon fuel, resulting in partial, selective, or complete oxidation. This process leads to phase transition and creates oxygen vacancies on the Fe-OC, which can significantly alter its morphology, chemical properties, and electronic structures. It also facilitates the transport of lattice O atoms from the bulk of the Fe-OC to the surface. Cheng *et al.* conducted DFT simulations to study the effect of oxygen vacancy on  $\text{CH}_4$  combustion using  $\text{Fe}_2\text{O}_3$  as an OC. They stated that the presence of oxygen vacancies significantly increases the  $\text{CH}_4$  activation on the Fe-OC by lowering the dissociation barrier for the C-H bond of the  $\text{CH}_4$  molecule.<sup>60</sup> During the oxidation reaction of Fe-OC in the absence of oxygen vacancies, the interstitial diffusion energy barrier for O moving inward is higher than the outward diffusion energy barrier of Fe, as shown in Fig. 3(a). This leads to a rapid formation of a  $\text{Fe}_2\text{O}_3$  layer on the outer surface of the Fe-OC particle due to the reaction between outward diffusing Fe ions and oxidant.



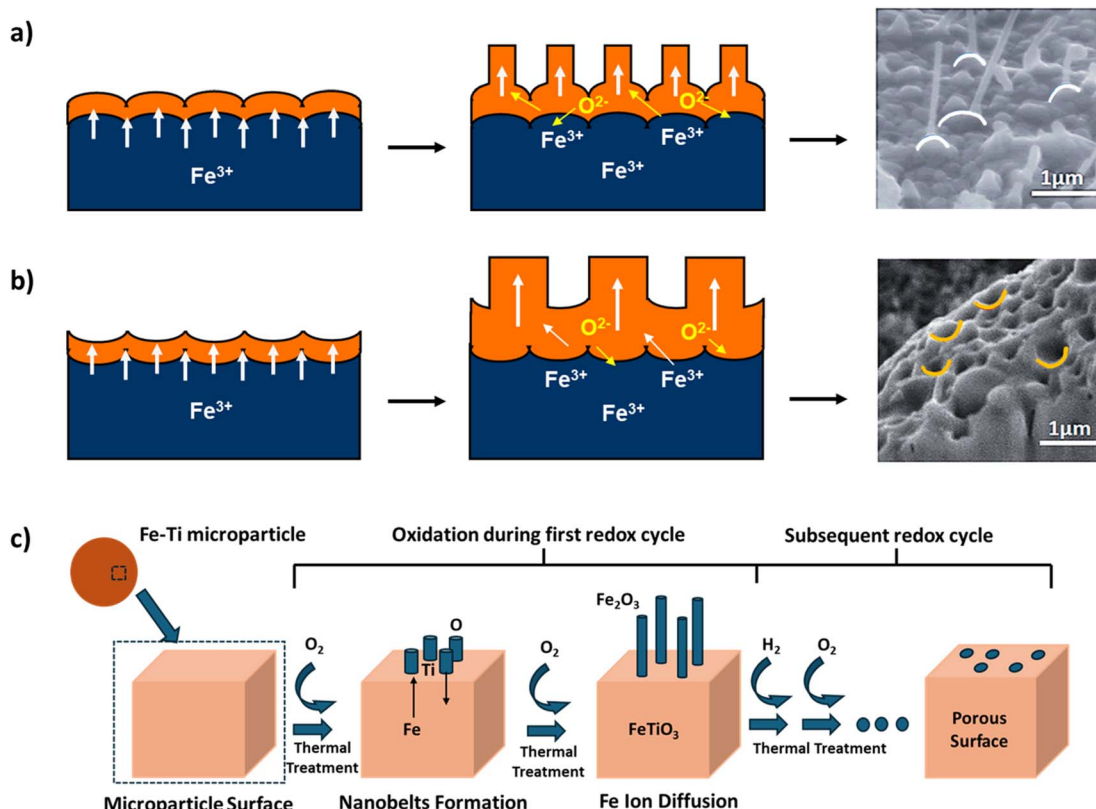


Fig. 2 Nanoscale morphological transformations showing growth mechanisms for (a) nanowires, (b) nanopores of ferrite material, and (c) iron oxide nanobelt formation in Fe-Ti composite. White curves in (a) indicate a positive curvature, while yellow curves in part (b) highlight the negative curvature on the surface. (a) and (b) Adapted with permission from ref. 58. Copyright 2014 Royal Society of Chemistry. (c) Adapted with permission from ref. 59. Copyright 2015 Royal Society of Chemistry.

However, the high energy barrier for O diffusion decreases the rate of oxidation within the particle bulk. In the presence of oxygen vacancies, the inward diffusion barrier of O is reduced. It is slightly lower than the outward diffusion barrier for Fe, as observed from Fig. 3(b), thus facilitating the formation of iron oxide product at the  $\text{Fe}_2\text{O}_3$ –Fe interface. This results in a rapidly progressing  $\text{Fe}_2\text{O}_3$  layer towards the center of the Fe-OC, enabling faster reaction rates for complete oxidation.<sup>57</sup>

Numerous atomistic studies on Fe-OCs have explored how dopants and support modifications can lower oxygen vacancy formation energy ( $\Delta E_{\text{vac}}$ ) to enhance lattice oxygen transport and redox activity. Modifying  $\text{Fe}_2\text{O}_3$  with  $\text{TiO}_2$  support decreases  $\Delta E_{\text{vac}}$ , enhancing the oxygen atom diffusion and substantially increasing the recyclability of the Fe-Ti composite OC.<sup>60</sup> The addition of 5% Ni dopant to  $\text{Ca}_2\text{Fe}_2\text{O}_5$  lowers  $\Delta E_{\text{vac}}$  by 58%, resulting in a substantial improvement of nearly 1149% in the Fe-OC's redox activity.<sup>61</sup> In another study, it was observed that doping  $\text{Fe}_2\text{O}_3$  with 1% Cu and 2% Co reduces  $\Delta E_{\text{vac}}$  by 29% and 31%, respectively.<sup>62,63</sup> Composite Fe-OCs have also been utilized in CLC applications. For example, adding  $\text{CeO}_2$  to  $\text{Fe}_2\text{O}_3$  OC significantly reduces  $\Delta E_{\text{vac}}$  from 9.56 eV (in pure  $\text{Fe}_2\text{O}_3$ ) to 3.95 eV (in the  $\text{CeO}_2/\text{Fe}_2\text{O}_3$  composite OC). This facilitated the increase in the formation of surface oxygen vacancies, improving the composite material's performance compared to pure  $\text{Fe}_2\text{O}_3$ .<sup>64</sup>

### 2.3. Structural design for enhanced Fe-OC performance

The reactivity and stability of Fe-OCs can be significantly enhanced by modifying their structural design, with core–shell structures showing promise in CL applications. Core–shell structures often form during redox cycles through solid–solid reactions between the active material and an inert support. During these cycles, cations diffuse outward, transporting the active material from the core to the surface, forming a protective shell around the core. The sol–gel method is one of the major preparation techniques that enable the synthesis of core–shell OCs with controlled composition and structure, making them well-suited for CL applications.<sup>65–67</sup>

Core–shell structures often outperform homogeneous composite materials. Ma *et al.* found that  $\text{Fe}_2\text{O}_3@\text{CeO}_2$  core–shell OC exhibited significantly higher redox reactivity and stability compared to  $\text{Fe}_2\text{O}_3/\text{CeO}_2$  homogeneous composite Fe-OC in CLHG applications. This improvement was due to the core–shell structure's strong resistance to sintering, which prevents Fe cations from migrating to the particle surface, thus maintaining the OC's stability and performance. In contrast, the homogeneous composite OC suffers from significant sintering, with Fe cations accumulating on the surface, leading to reduced performance.<sup>68</sup> The careful design of both core and shell materials is essential for superior CL performance.



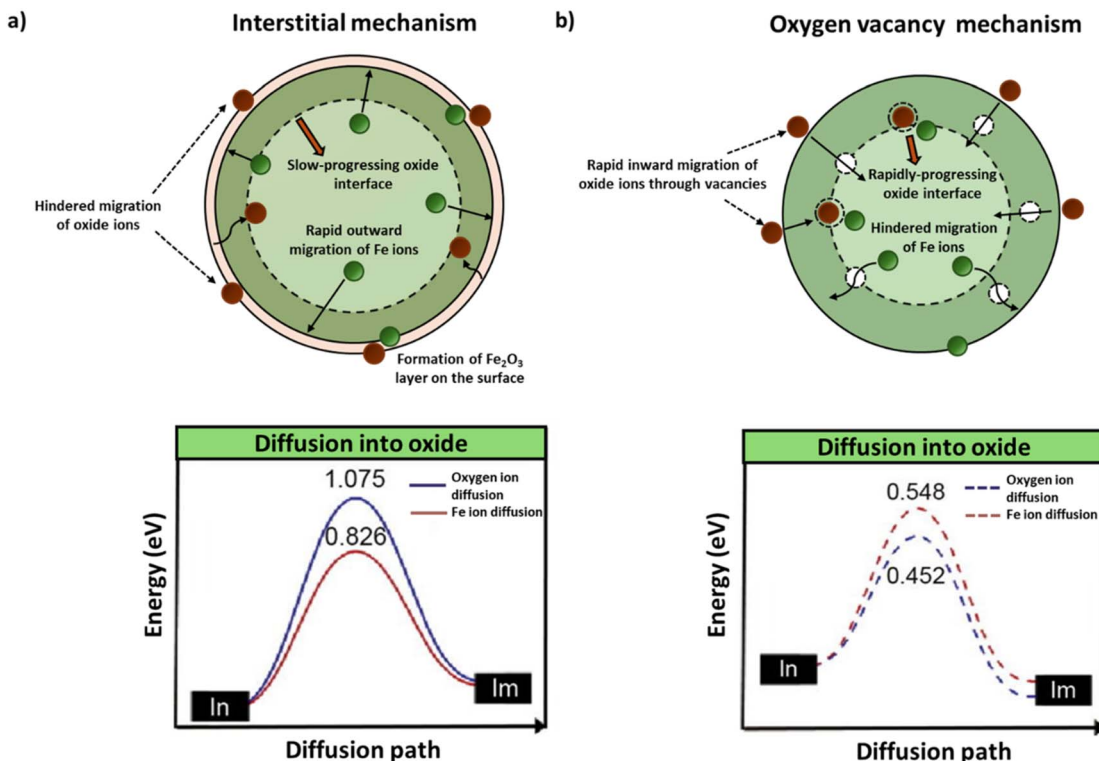


Fig. 3 Ionic diffusion and corresponding activation energy diagram for  $\text{Fe}_2\text{O}_3$  OC under (a) interstitial mechanism. (b) Vacancy mechanism. Green and white spheres indicate Fe ions and oxide ions, respectively, while white spheres depict oxygen vacancies. Energy diagrams adapted from a 2018 article published by Elsevier (ref. 57) under a CC BY-NC-ND 4.0 License.

Blaschke *et al.* studied the impact of shell composition on the performance of OCs by using  $\text{Fe}_2\text{O}_3$  as the core and preparing two samples with different shell compositions: yttrium-stabilized zirconium oxide with 8 mol%  $\text{Y}_2\text{O}_3$  (YSZ8-CS) and yttria-stabilized zirconium oxide with over 10 mol%  $\text{Y}_2\text{O}_3$  (YSZ10-CS). The ratio of weights of  $\text{Fe}_2\text{O}_3$  and the support YSZ was kept constant. Both samples show increased pore volume during redox cycles, but YSZ10-CS develops poorly connected pores, reducing effective porosity and leading to sintering and agglomeration. In contrast, YSZ8-CS maintains a stable pore structure, avoiding “ink bottle” pores that trap gases, thereby preserving its effectiveness and overall performance.<sup>69</sup> Yin *et al.* investigated  $\text{Fe}_2\text{O}_3$  nanocores covered with a  $\text{CeO}_2$  shell. This configuration combined the superior ion conductivity of  $\text{CeO}_2$  with the high oxygen storage capacity of  $\text{Fe}_2\text{O}_3$ . The resulting Fe–Ce core–shell OC was highly influential in selectively providing oxygen from the  $\text{CeO}_2$  shell, which improved selectivity towards syngas production and enhanced  $\text{CH}_4$  conversion.<sup>70</sup>

### 3 Prominence of Fe-OCs in CL processes

Understanding the fundamental properties of the materials and their impact on the performance of the OC provides a strong foundation for exploring the Fe-OCs for various CL applications for carbon neutrality and clean energy production. The choice

of active component greatly dominates the feasibility of the CL process. This section dwells on the thermodynamic feasibility, experimental evaluation, and scale-up studies of Fe-OCs for different CL applications.

#### 3.1. Thermodynamic feasibility of oxygen release and uptake by Fe-OC

Fe-OCs have enabled the application of CL technology to produce a wide range of commodity chemicals. However, the thermodynamics of the Fe-OC during the oxidation and reduction reactions dictate the feasibility of the desired CL application. CLC, CLPO, and CLHG are the prominently pursued CL applications in the literature for achieving clean and sustainable energy production.

Thermodynamic feasibility is influenced by several factors, including fuel conversion,  $\text{CO}_2$  purity, syngas purity, and product selectivity. In a commercial-scale CL process, oxygen carriers must favor complete thermodynamic fuel conversion while maintaining high selectivity toward the target product. Additionally, the kinetic activity of Fe-OCs should facilitate fuel conversion and product selectivity approaching thermodynamic limits. With the increasing emphasis on renewable feedstocks such as biomass, these properties become even more critical for achieving complete tar cracking and ensuring high product yields. The study of the Ellingham diagram presents a useful approach for determining the viability of the Fe-OC for a given CL process by evaluating the oxidation potential of the carrier.



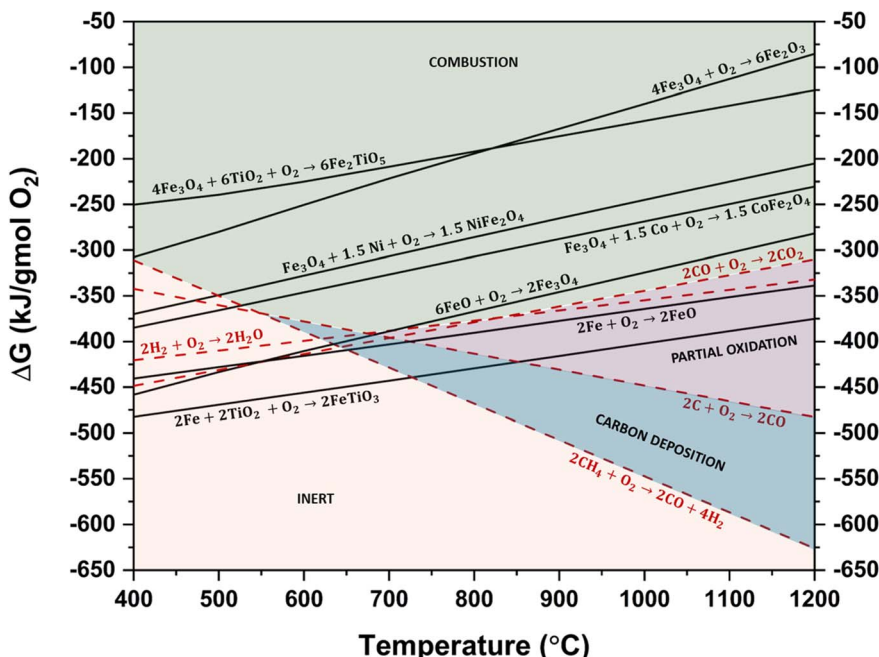


Fig. 4 Ellingham diagram for various metal ferrite OCs.

Fig. 4 illustrates the Ellingham diagram for some prominent Fe-OCs. The free energy of oxidation of the reduced counterparts of the Fe-OCs indicates the thermodynamic feasibility of  $\text{Fe}_2\text{TiO}_5$ ,  $\text{NiFe}_2\text{O}_4$ ,  $\text{CoFe}_2\text{O}_4$ ,  $\text{Fe}_2\text{O}_3$ , and  $\text{Fe}_3\text{O}_4$  for CLC application, while  $\text{FeO}$  and  $\text{FeTiO}_3$  can establish equilibrium with syngas during CLPO application.<sup>43,71,72</sup> While this theoretical assessment indicates if a particular process is thermodynamically favored, an experimental examination is necessary to assess the kinetics and oxygen transport capacity (OTC) of the Fe-OC material. Therefore, the experimental evaluations are studied in Section 3.2 to investigate the practical application of Fe-OC for CL processes.

### 3.2. Experimental evaluation of Fe-OC for diverse CL processes

In order to enable complete carbon capture during the CLC process, it is essential to utilize materials with high oxygen transport capacity, similar to  $\text{Fe}_2\text{O}_3$ , which has a theoretical OTC of 30.06%. As observed in Section 3.1, Fe-OCs, such as  $\text{CoFe}_2\text{O}_4$ , exhibit a high oxidation potential and demonstrate a high theoretical OTC of 27.28%. With the OTC being similar to  $\text{Fe}_2\text{O}_3$  and thermodynamics favoring complete combustion,  $\text{CoFe}_2\text{O}_4$  has been extensively examined for CLC application. Evaluation conducted by Fan and co-workers to synthesize OC with high OTC using Cu, Fe, and Mn as constituent metals revealed the notable performance of  $\text{CuFeMnO}_4$  Fe-OC for CLC, owing to the theoretical OTC of 20.04%, synergistic effect of the trimetallic system, and distinct reaction profile.<sup>73,74</sup> Composite OC like  $\text{NiFe}_2\text{O}_4$  also exhibits a high theoretical OTC of 27.31%, allowing complete carbon capture and improved tar cracking properties arising from the high

catalytic activity of the metallic Ni formed in the reduced phase and unique spinel structure.<sup>72,75</sup>

As opposed to CLC, where a higher OTC is favored, materials with a lower oxidation potential and lower OTC than  $\text{Fe}_2\text{O}_3$  are promising for CLPO.  $\text{Ca}_2\text{Fe}_2\text{O}_5$ , having a low theoretical OTC of 17.66%, has revealed high conversions and remarkably high syngas selectivity, as showcased by Shah *et al.*<sup>61</sup> More than 99%  $\text{CH}_4$  conversion with >98% syngas selectivity obtained can be ascribed to the brownmillerite type structure and favorable thermodynamics of oxygen transfer for partial oxidation. Moreover, the ability of  $\text{Ca}_2\text{Fe}_2\text{O}_5$  to regenerate using  $\text{CO}_2/\text{H}_2\text{O}$  increases the overall syngas yield.<sup>76</sup> Other probable candidates for CLPO applications, such as  $\text{Li}_5\text{FeO}_4$ ,  $\text{SrFe}_{12}\text{O}_{19}$ , *etc.*, with a maximum OTC of 12.13% and 23.73%, respectively, possess bifunctional properties with both catalytic and oxygen transfer properties.<sup>77,78</sup> The Fe-Ti-based synthetic OC developed by Ohio State University (OSU) has shown excellent syngas yield due to its oxygen migration control, achieving syngas purities as high as 90%.<sup>43,47</sup> While theoretical OTC helps identify the potential CL application for Fe-OC, it is important to note that the thermodynamics and kinetic activity of the Fe-OC play a crucial role in determining actual OTC and the product selectivity, as seen in the case of  $\text{SrFe}_{12}\text{O}_{19}$ .

CLHG processes are commonly combined with CLC or CLPO, where the oxidizer produces  $\text{H}_2$  by steam oxidation of the OC. The favorable thermodynamics of OC for steam regeneration are an essential prerequisite for its use in CLHG. The  $\text{H}_2$  yield from the material highly depends on the degree of reduction of Fe-OC, which is higher in CLC than in CLPO. Thus, to maximize the yield of  $\text{H}_2$ , CLC followed by the CLHG process was studied using metal ferrites like  $\text{CaFe}_2\text{O}_4$ ,  $\text{Co}_{0.85}\text{Fe}_{2.15}\text{O}_3$ ,  $\text{NiLa}_{0.2}\text{Fe}_{1.8}\text{O}_4$ , *etc.*, which display higher redox stability over

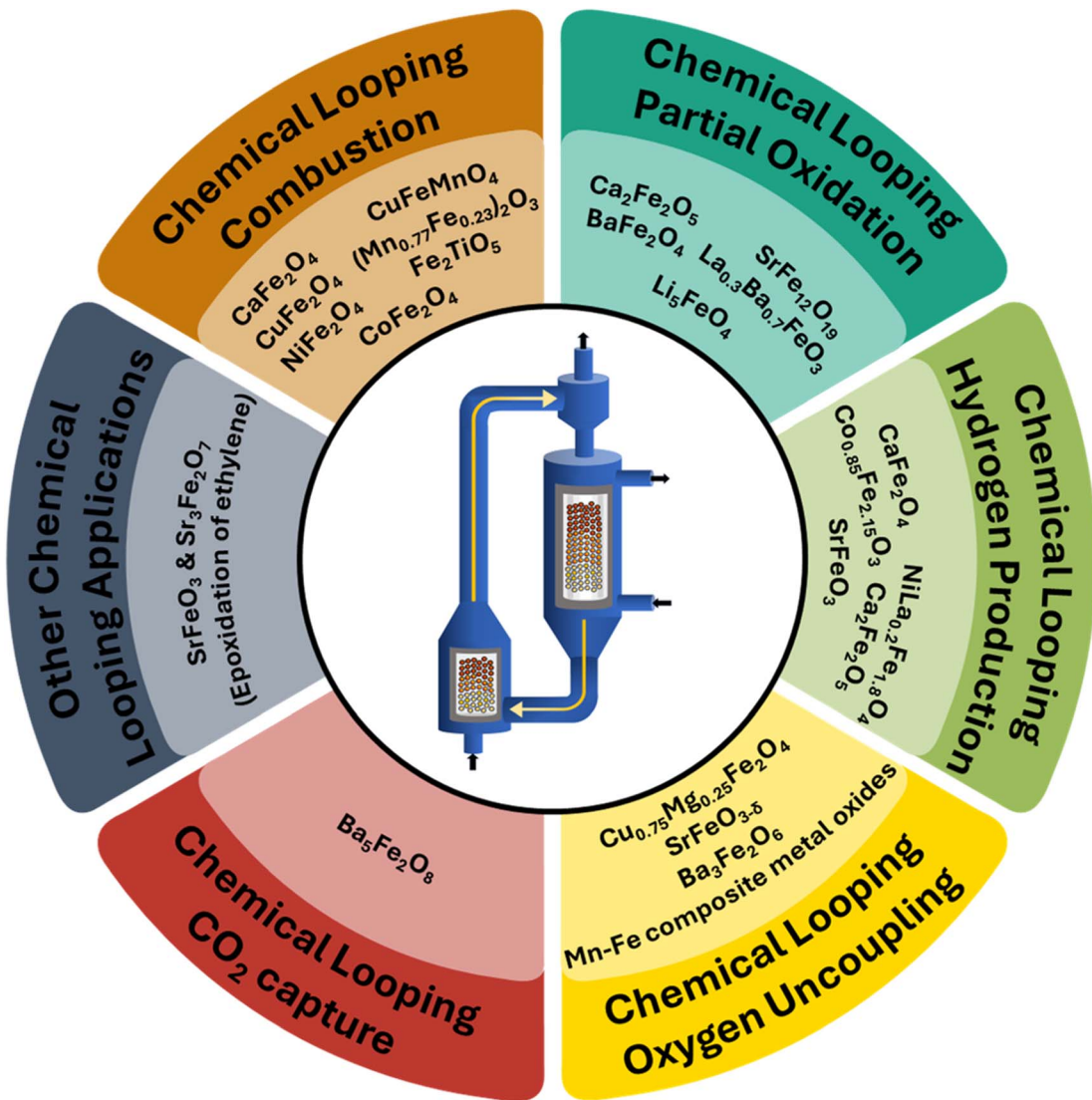


Fig. 5 Application of ferrites in different CL processes. The central CL unit adapted from a 2024 article published by Elsevier (ref. 20) under a Creative Commons Attribution 4.0 International (CC BY 4.0) License.

Fe<sub>2</sub>O<sub>3</sub>.<sup>79–82</sup> At the same time, the ability of Ca<sub>2</sub>Fe<sub>2</sub>O<sub>5</sub> to regenerate completely using steam has made it a promising candidate for syngas-H<sub>2</sub> co-generation.

Apart from the conventional applications of the CL processes, several OCs have been developed for applications such as CLOU, oxidative dehydrogenation, preferential oxidation, selective dehydrogenation, *etc.*, as summarized in Fig. 5. SrFeO<sub>3</sub> and Sr<sub>3</sub>Fe<sub>2</sub>O<sub>7</sub> in a 1:1 ratio have been utilized for chemical looping ethylene epoxidation and have shown significantly higher yields of ethylene oxide as compared to conventional processes.<sup>83–85</sup> Controlled oxidation enables a four times higher yield than conventional processes due to its property of controlled oxidation. Similarly, a mixture of Ba<sub>5</sub>Fe<sub>2</sub>O<sub>8</sub> and Ba<sub>3</sub>Fe<sub>2</sub>O<sub>6</sub> can be utilized for CLOU with inherent CO<sub>2</sub> capture at high temperatures, leveraging the superior capture performance of the former and higher oxygen uncoupling of the latter. Table 1 summarizes details on the structure, method of preparation, and applications of some Fe-OCs.

### 3.3. Performance evaluation of Fe-OC for scaled-up CL applications

With a realization of the scale-up potential of various Fe-OCs, various demonstrations on bench-scale, sub-pilot scale, and pilot scale have been conducted, highlighting the capability of chemical looping technology for clean energy production and achieving carbon neutrality. This section draws attention to the scale-up attempts of CL spanning from kW<sub>th</sub> to MW<sub>th</sub> scale using synthetic and natural Fe-OCs for diverse feedstocks.<sup>99</sup>

Southeast University has experimentally investigated CLC in continuous fluidized bed reactors ranging from a scale of 1–50 kW<sub>th</sub> for a wide range of solid fuels using synthetic Fe-OC.<sup>100–103</sup> These tests proved the potential of Fe-OC as a low-cost carrier for commercial coal-fueled CLC units. OSU demonstrated a 25 kW<sub>th</sub> followed by a 250 kW<sub>th</sub> high-pressure moving bed reactor configuration for syngas utilization using Fe-Ti OC to enable H<sub>2</sub> production with 100% CO<sub>2</sub> capture.<sup>46</sup> Another 250 kW<sub>th</sub>

Table 1 Classification of Fe-O-C based on phases and the effects observed on CL processes due to different preparation methods and experimental conditions

OC	Preparation method	Experimental temperature	Application	Key findings	Ref.
<b>Spinel</b> NiFe <sub>2</sub> O <sub>4</sub>	Sol-gel	800 °C	CLHG	Grain coalescence and surface densification lead to deactivation, which can be prevented by incorporating Al	86
Cu <sub>x</sub> Mg <sub>1-x</sub> Fe <sub>2</sub> O <sub>4</sub>	Mechanical mixing and calcination	900–1000 °C	CLC	~98.9% conversion of waste biomass	84
M <sub>x</sub> Fe <sub>3-x</sub> O <sub>4</sub> , M = Cr and Mn	Iron ore	850 °C	CLC	The addition of Mg improved crushing strength above 157.19 MPa	87
Cu <sub>x</sub> Mn <sub>1-x</sub> Fe <sub>2</sub> O <sub>4</sub>	Co-precipitation	600–700 °C	CL-SMR	Fe-Cr-based OC demonstrates improved stability and performance due to the spinel structure	87
Cu <sub>0.2</sub> Co <sub>0.8</sub> Fe <sub>2</sub> O <sub>4</sub>	Sol-gel	<750 °C	CL-CO <sub>2</sub> splitting	Cu <sub>0.6</sub> Mn <sub>0.4</sub> Fe <sub>2</sub> O <sub>4</sub> enabled CH <sub>4</sub> conversion of ~98.7% and H <sub>2</sub> yield of ~81.02%	88
				Improved reduction facilitated by Cu and Co as co-dopants	89
				Increasing Cu doping results in the formation of impurities detrimental to the CO <sub>2</sub> -splitting process	
<b>Petroskite</b> La <sub>0.75</sub> Sr <sub>0.25</sub> FeO <sub>3</sub> -encapsulated Co <sub>3</sub> O <sub>4</sub> -NiO	Modified Pechini	600 °C	CL-RWGS	Promotes oxygen defects in the metal oxide core during H <sub>2</sub> -CO <sub>2</sub> redox cycles, enabling higher yield of CO	90
La <sub>0.5</sub> Sr <sub>0.5</sub> Fe <sub>0.5</sub> Co <sub>0.5</sub> O <sub>3-δ</sub>	Glycine-nitrate combustion and spray drying	900 °C	CLC	La substitution increases the OTC	91
La <sub>1-x</sub> Sr <sub>x</sub> FeO <sub>3</sub>	Sol-gel	1000 °C	CLR	The selectivity towards CO/H <sub>2</sub> and the reactivity with CH <sub>4</sub> was reduced	92
				Partial substitution of La <sup>3+</sup> by Sr <sup>2+</sup> causes electronic imbalance, which is compensated by oxidation of a fraction of Fe <sup>3+</sup> to Fe <sup>4+</sup> and/or generation of oxygen vacancies	
				The optimum range of the degree of Sr substitution is $x = 0.3-0.5$	
LaFe <sub>1-x</sub> Co <sub>x</sub> O <sub>3</sub>	Combustion	850 °C	CLR	The surface adsorbed oxygen essential for complete oxidation of CH <sub>4</sub> increases with Co substitution	93
Sr(Fe <sub>1-x</sub> Cu <sub>x</sub> )O <sub>3-δ</sub>	Calcination method	600–800 °C	CLC	The optimum degree of Co substitution is $x = 0.3$	94
				Can sustain very high temperatures (>1280 °C) with a crushing strength >39.32 MPa	
<b>Pseudobrookite</b> Fe <sub>2</sub> TiO <sub>5</sub>	Mechanical mixing followed by pulverization	875–925 °C	CLC	Improved diffusion of CH <sub>4</sub> through the Fe-OC led to an enhanced activity of Fe <sub>2</sub> TiO <sub>5</sub> supported on Al <sub>2</sub> O <sub>3</sub>	95
<b>Brownmillerite</b> Ca <sub>2</sub> Ni <sub>0.25</sub> Fe <sub>1.75</sub> O <sub>5</sub>	Sol-gel	900 °C	CL-SR	Ni induces structural changes to the brownmillerite lattice, increasing the distortion of the FeO <sub>6</sub> octahedra. The structural changes lead to improved lattice oxygen activity	96
Ca <sub>2</sub> Fe <sub>2</sub> O <sub>5</sub>	Sol-gel	850 °C	CL-SR	Reduction of the migration energy barrier of lattice oxygen between bulk and surface improved the reactivity	97
MgO supported Ca <sub>2</sub> Fe <sub>2</sub> O <sub>5</sub>	Solid state synthesis	1000 °C	CLR	CO <sub>2</sub> counter-oxidation enabled ~20% higher CO <sub>2</sub> utilization compared to tri-reforming	98

Table 2 A non-exhaustive list of scale-up attempts for CL processes with Fe-OC

Fe-OC	Feedstock	Hours of operation	Scale	Reactor configuration	Ref.
<b>Synthetic iron-based</b>					
Fe <sub>2</sub> O <sub>3</sub> -supported	Coal, biomass	200–600	25–250 kW <sub>th</sub>	Moving bed	44, 48 and 121
Fe <sub>2</sub> O <sub>3</sub> and Fe <sub>2</sub> O <sub>3</sub> /Al <sub>2</sub> O <sub>3</sub>	Biomass	30, 60	10 kW <sub>th</sub>	Fluidized bed	105 and 122
Fe–Ni and Fe–Cu on Al- and MgAl-based supports	Natural gas, biomass, coke oven gas	2–40	10–50 kW <sub>th</sub>	Fluidized bed	106, 107, 123 and 124
<b>Natural ore based</b>					
Iron ore	Biomass and coal	26	100 kW <sub>th</sub>	Fluidized bed	125
Ilmenite	Coal, petcoke, biomass, CH <sub>4</sub> , CO, and H <sub>2</sub>	22–160	10 kW <sub>th</sub> –12 MW <sub>th</sub>	Fluidized bed	113–115 and 126–129
Ilmenite–iron ore	Coal and biomass	110	1 MW <sub>th</sub>	Fluidized bed	119
Hematite	Coal	100	5 kW <sub>th</sub>	Fluidized bed	116
Ilmenite–manganese ore	Biomass and petcoke	18	100 kW <sub>th</sub>	Fluidized bed	130

demonstration highlighted the supremacy of Fe–Ti OC for near 100% conversion of direct solid fuels.<sup>48</sup> Over 600 hours of testing using Fe-OC for biomass gasification in a 25 kW<sub>th</sub> sub-pilot unit exhibited excellent tar-cracking capabilities, high attrition resistance, and stable reactivity of the Fe–Ti OC for extended redox operation.<sup>44</sup>

Incorporating additional metal oxides, such as CuO and NiO, into Fe-OCs has demonstrated the potential to enhance their reactivity while maintaining cyclic stability, positioning these OCs as promising candidates for the scale-up of CL technology.<sup>104</sup> In a 10 kW<sub>th</sub> demonstration for biomass gasification, Fe–Ni bimetallic OCs improved the gasification efficiency compared to single metal OC owing to the catalytic activity of Ni.<sup>105,106</sup> Investigations conducted in a 10 kW<sub>th</sub> and 50 kW<sub>th</sub> CLC unit using coke oven gas and CH<sub>4</sub>, respectively, established the superiority of supported Cu–Fe OC for extended redox testing and for the achievement of autothermal operation.<sup>107–109</sup>

Besides synthetic Fe-OC, natural ores have gained attention for CL applications owing to their low cost and excellent sintering resistance. Experimental evaluation in 10 kW<sub>th</sub> and 100 kW<sub>th</sub> by Chalmers University using ilmenite and a mixture of ilmenite–hematite demonstrated high fuel conversion for low-volatile solids with a projected Fe-OC lifespan of 700–800 hours.<sup>110–115</sup> Natural mineral-based OCs, like hematite, have also been evaluated in fluidized bed CLC reactors.<sup>116</sup> 25 kW<sub>th</sub> scale CLG investigation for coal and biomass achieved high syngas purity with high carbon conversion.<sup>117</sup> A CLC plant on a 1 MW<sub>th</sub> scale at Technische Universität Darmstadt demonstrated auto-thermal operation for coal CLC using both ilmenite and hematite.<sup>118–120</sup> These commercial-scale demonstrations show that natural iron ores could be a suitable material with good mechanical properties, low attrition, good reactivity, high OTC, and low cost. Table 2 provides a further overview of some of the scale-up attempts for CL technology reported in the literature.

## 4 Challenges and opportunities

In order to implement the potential benefits of the CL systems on a commercial scale, the ability of the Fe-OC to maintain

reactivity and structural stability over an extended period of testing is crucial. This section highlights some of the key challenges encountered in the use of Fe-OCs for CL applications. Moreover, detailed insight into plausible composition modifications, which can ameliorate the barriers to the implementation of Fe-OC on a commercial scale, has been discussed.

### 4.1. Cyclic stability and active material dispersion of Fe-OC

Fe-OCs face a significant challenge in maintaining cyclic stability during the redox process owing to poor mechanical strength and active site dispersion on the OC, which can be improved by the incorporation of inert support material. Common supports that have demonstrated an improvement in the material stability for extended redox cycles include but are not limited to Al<sub>2</sub>O<sub>3</sub>, TiO<sub>2</sub>, ZrO<sub>2</sub>, YSZ, CaO, MgO, and CeO<sub>2</sub>. A reactivity improvement in the order of Al<sub>2</sub>O<sub>3</sub> > SiO<sub>2</sub> > TiO<sub>2</sub> > unsupported > CaO is observed in Fe<sub>2</sub>O<sub>3</sub>, which could be attributed to the enhanced gas diffusion through the interconnected pores in Al<sub>2</sub>O<sub>3</sub>, SiO<sub>2</sub>, and TiO<sub>2</sub>-supported OCs. Moreover, Al<sub>2</sub>O<sub>3</sub> and TiO<sub>2</sub> also contribute to the increase in mechanical strength of the Fe-OC during the fluidized bed testing.<sup>131</sup> Tijani *et al.* found that the use of ZrO<sub>2</sub> and CeO<sub>2</sub> supports significantly decrease the activation energy barrier by ~4 times during the oxidation step compared to Al<sub>2</sub>O<sub>3</sub> and TiO<sub>2</sub>.<sup>132</sup> In order to prevent the eventual loss of reactivity by using CeO<sub>2</sub> support, the Fe–Ce structure was stabilized by adding ~7 wt% of ZrO<sub>2</sub> in the fluorite configuration of CeO<sub>2</sub>. This leads to the formation of oxygen vacancies and mitigates the formation of CeFeO<sub>3</sub>, increasing the redox stability of the Fe-OC.<sup>133</sup>

The active material dispersion and reactivity can be further enhanced using mesoporous inert supports like SBA-15 to synthesize nano-scaled carriers. Kumar *et al.* observed a remarkable 1000% improvement in reactivity using LaFeO<sub>3</sub>-SBA-15 compared to the bulk carrier for CLC application owing to the formation of a reactive cubic phase at the nanoscale.<sup>20</sup> Fe<sub>2</sub>O<sub>3</sub> nanoparticles synthesized by Liu and co-workers using the SBA-15 matrix for CLPO application display >99.3% selectivity toward CO formation from CH<sub>4</sub> and a stable performance



for 75 redox cycles. The 70% improvement in conversion rate and ~200% higher CO concentration compared to the bulk carrier can be attributed to the lower adsorption and dissociation energies of  $\text{CH}_4$  in the presence of nanoparticles.<sup>134</sup>

In addition to the choice of inert support, the synthesis technique used has a profound effect on the performance of Fe-OC in chemical looping. Mechanical mixing, freeze granulation, dry and wet impregnation, co-precipitation, and sol-gel are commonly practiced methods to prepare Fe-OCs.  $\text{Fe}_2\text{O}_3$ - $\text{Al}_2\text{O}_3$  OCs prepared by the sol-gel process in the Fe :  $\text{Al}_2\text{O}_3$  molar ratio of 2 : 1 demonstrate better reactivity and stable performance across multiple redox cycles, among other preparation methods like mechanical mixing and dipping.<sup>135</sup> This can be attributed to the excellent homogeneity and control over microstructure in the sol-gel method, which leads to the formation of  $\text{Al}_3\text{Fe}_5\text{O}_{12}$ .<sup>28</sup> Another study identified that the conventional wet impregnation method for preparing Fe-OCs is challenged by poor dispersion of active material on the support and insufficient penetration into the binder material. However, this challenge was resolved using the ultrasonic wet impregnation technique, characterized by a reduction in the crystalline size and better dispersion of the active material, enabling higher conversions of  $\text{CH}_4$ .<sup>136</sup>

#### 4.2. Loss of reactivity and performance degradation

The incorporation of inert support enhances the cyclic stability of the material. However, a decrease in the performance of the Fe-OC has been observed with increasing redox cycles, arising due to degradation in the OTC.<sup>137</sup> Dopant modification is an effective technique to retain the reactive capability of the Fe-OC

over an extended number of cycles. Alkaline metals are commonly studied as dopants since they act as an electron donor and weaken the Fe-O bond. Liu *et al.* observed that 2.6 mol% K doped Fe-Al carrier demonstrates superior  $\text{CO}_2$  selectivity and stable reactivity for ~50 redox cycles. This can be ascribed to the stiffening of the  $\text{Al}_2\text{O}_3$  matrix in the presence of K, providing a stable path for [O] migration.<sup>137</sup> Similarly, adding 5% Na using sodium salt, like NaCl, as a dopant in the Fe-Al matrix also helps increase the yield of  $\text{CO}_2$  in CLC.<sup>138</sup> Isovalent metal oxide dopants like 1% La dramatically enhance the reactivity for the combustion of CO and regeneration by ~233% and 266%, respectively. This can be attributed to the lowering of the energy barrier due to La for CO bond activation.<sup>139</sup> Doping 2% La on Fe- $\text{CeO}_2$ -based OC results in the Fe- $\text{La}_{0.02}\text{Ce}_{0.95}\text{O}_{1.99}$  phase, facilitating a very high oxygen transport by altering the thermodynamic stability of  $\text{CeO}_2$ . Increasing the dopant concentration beyond 10% does not contribute significantly to further enhancement owing to La phase separation to form  $\text{LaFeO}_3$  with poor reactivity. The cyclic stability testing with 10% La doping on the  $\text{CeO}_2$  matrix results in the formation of Fe- $\text{La}_{0.1}\text{Ce}_{0.9}\text{O}_{1.95}$ . La-doped Fe-OC demonstrated excellent recyclability over 50 redox cycles, whereas the undoped Fe-OC lost the ability to regenerate after 11 cycles.<sup>140</sup>

#### 4.3. Carbon and ash deposition

Carbon deposition can significantly compromise the Fe-OC stability and purity of the products, which may negate the inherent product separation advantage of CL systems. Carbon can exist in amorphous, filamentary, and crystalline graphitic

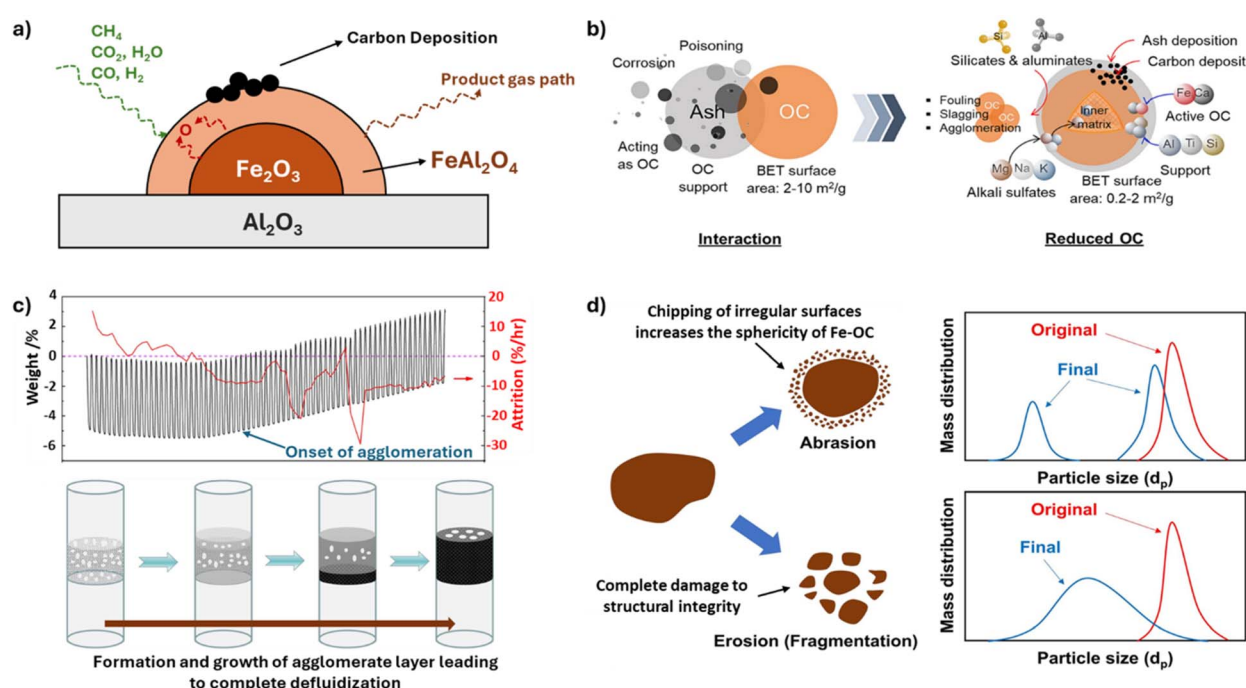


Fig. 6 Challenges encountered in CL applications while using Fe-OC. (a) Onset of carbon deposition. Adapted with permission from ref. 149. Copyright 2023 Elsevier. (b) Ash deposition. Adapted from article (ref. 150) published by Elsevier under a Creative Commons Attribution 4.0 International (CC BY 4.0) License. (c) Formation and growth of agglomerate layer. Adapted with permission from ref. 151. Copyright 2023 Elsevier. (d) Fe-OC attrition. Adapted with permission from ref. 152 and 153. Copyright 2016 and 2023 Elsevier.



forms and get deposited on the Fe-OC particles.<sup>141,142</sup> Deeply reduced Fe-OCs are susceptible to carbon deposition owing to the difficulty in lattice oxygen migration through the metallic Fe and FeO phases.<sup>143,144</sup> The two major strategies to prevent carbon deposition are (1) dopant and support modification to mitigate the C-H bond cleavage. (2) Synthesis of composite metal oxides to increase the lattice oxygen mobility for enhancing the oxidation of deposited carbon.

Modifying the natural iron ore-based OC by adding alkali metal, Ni, and Cu-based dopants blocks the active sites for carbon accumulation and increases the mobility of lattice oxygen by alleviating the iron–oxygen interaction. MgO modification, 10% KNO<sub>3</sub> decoration, and co-doping of K and Cu can improve the ability to remove carbon by enhancing oxygen mobility for natural Fe-OCs.<sup>145–148</sup> Synthetic Fe-Al OCs face the challenge of carbon deposition owing to the increase in acidic sites, which enhances C-H bond cleavage and the formation of FeAl<sub>2</sub>O<sub>4</sub> spinel with low [O] mobility, as shown in Fig. 6(a).<sup>154,155</sup> K<sub>2</sub>CO<sub>3</sub>-doped Fe-Al-based OCs have demonstrated the prevention of carbon deposition by limiting the concentration of acidic sites. Y-Doped Fe-Al OCs sintered at 1200 °C form a garnet structure Y<sub>3</sub>Fe<sub>x</sub>Al<sub>5-x</sub>O<sub>12</sub> ( $x = 1, 2, 3$ ), demonstrating high selectivity for syngas production by avoiding carbon deposition.<sup>156,157</sup> Adding MgO in Fe-Al OCs gives rise to the phase of MgAl<sub>2</sub>O<sub>4</sub>, which mitigates the interaction between iron oxide and Al<sub>2</sub>O<sub>3</sub>, reducing carbon deposition.<sup>158</sup> CeO<sub>2</sub>-Modified Al<sub>2</sub>O<sub>3</sub> support, or Fe<sub>2</sub>O<sub>3</sub> supported on 40% CeO<sub>2</sub>, leads to the formation of a perovskite CeFeO<sub>3</sub> structure that can generate channels for [O] migration, eliminating carbon accumulation on OC.<sup>52,68,159–161</sup> Besides dopant and support modification, iron-based composites are known to enhance the reactivity and alleviate carbon deposition. Spinel structures like CuFe<sub>2</sub>O<sub>4</sub>, BaFe<sub>2</sub>O<sub>4</sub>, 4% Cu-4% Ce doped CoFe<sub>2</sub>O<sub>4</sub>, and 70% CeO<sub>2</sub>-NiFe<sub>2</sub>O<sub>4</sub> have demonstrated microstructural integrity over multiple redox cycles and facilitated higher [O] release to prevent carbon deposition.<sup>104,162–168</sup> Perovskite structures like La<sub>0.5</sub>Ce<sub>0.5</sub>FeO<sub>3</sub>, BaFe<sub>0.4</sub>Sn<sub>0.6</sub>O<sub>3- $\delta$</sub> , and LaSrFe<sub>2-x</sub>Co<sub>x</sub>O<sub>6</sub> improve the reactivity and mitigate carbon deposition owing to increased oxygen migration due to structural distortion.<sup>169</sup> Hexaaluminates like BaFe<sub>x</sub>Al<sub>12-x</sub>O<sub>19</sub> and LaFe<sub>3</sub>Al<sub>5</sub>-O<sub>19</sub> have proved to be promising candidates for OC with low coking and high reactivity.<sup>170,171</sup>

Solid feedstocks, including fossil fuels like coal, sustainable carbon sources like biomass, and non-conventional feedstocks like municipal waste, present a challenge of ash deposition, as illustrated in Fig. 6(b). The components in ash include SiO<sub>2</sub>, Al<sub>2</sub>O<sub>3</sub>, Fe<sub>2</sub>O<sub>3</sub>, CaO, TiO<sub>2</sub>, K<sub>2</sub>O, MgO, Na<sub>2</sub>O, and P<sub>2</sub>O<sub>5</sub>. While the effects of ash deposition are not completely adverse, they can cause physical damage to the Fe-OC particles by clogging the pores, resulting in loss of reactivity and inducing mechanical stresses, leading to crack formation in the particles.<sup>172,173</sup> Chemical interactions between fuel and low melting components like Ca and K from ash can lead to agglomeration of the particles and corrosion of the CL equipment.<sup>150,174</sup> While ash majorly has detrimental effects on the Fe-OC, some active components present in the ash improve the reaction rate. Ca-based oxides in the ash prevent the formation of side products like Al- and Si- complexes, which are responsible for

deactivating the Fe-OCs. The oxides of transition metals in the ash enhance the redox stability, and components like Fe<sub>2</sub>O<sub>3</sub> and CaSO<sub>4</sub> promote the kinetic activity of the oxygen carrier.<sup>175</sup>

In order to tackle the deteriorating effects of the ash, some techniques like washing for removing soluble salts of K, Ca, Si, P, Cl, Mg, and Na and pickling to remove water-insoluble salts by acid treatment are well-known.<sup>176,177</sup> In addition to biomass pre-treatment, structural and compositional optimization to prevent the blocking of pores and improve redox activity can be beneficial in negating inhibitory effects like agglomeration and deactivation arising from ash deposition. NiFe<sub>2</sub>O<sub>4</sub>, MnFe<sub>2</sub>O<sub>4</sub>, CoFeAlO<sub>x</sub>, CuFe<sub>2</sub>O<sub>4</sub>, Ca<sub>2</sub>Fe<sub>1.8</sub>Co<sub>0.2</sub>O<sub>5</sub> are found to maintain excellent redox activity and mitigate agglomeration, which can subside the adverse effects observed due to ash deposition.<sup>178–180</sup>

#### 4.4. Durability of Fe-OC particles over long-term redox cycling

Due to the low Tamman temperatures ( $T_{\text{Tam}}$ ) of iron oxides, Fe-OCs tend to agglomerate, causing the deactivation of the OC and a decrease in oxygen diffusion. In moving and fluidized bed CL technologies, particle agglomeration can lead to reactor bridging and defluidization, which can hinder the long-term cyclic performance of the material, as shown in Fig. 6(c).

Some bimetallic Fe-OCs like CoFe<sub>2</sub>O<sub>4</sub>, Fe<sub>2</sub>TiO<sub>5</sub>, and Ca<sub>2</sub>Fe<sub>2</sub>O<sub>5</sub> have high melting points of  $\sim$ 1570 °C,  $\sim$ 1550 °C, and  $\sim$ 1450 °C, respectively correspondingly increasing  $T_{\text{Tam}}$ .<sup>181,182</sup> This helps the Fe-OCs to sustain higher operational temperatures, which can be beneficial for improving activity and thermodynamic conversions. Also, adding inert support ameliorates sintering as it increases the heat capacity of the material, thus raising the  $T_{\text{Tam}}$  of the Fe-OC. Cho *et al.* reported a stable performance of Fe<sub>2</sub>O<sub>3</sub>-Al<sub>2</sub>O<sub>3</sub> (2 : 3) particles for 40 cycles without defluidization due to agglomeration.<sup>183</sup> A bimetallic NiFe<sub>2</sub>O<sub>4</sub> carrier supported on a SiO<sub>2</sub> alleviates sintering compared to unsupported NiFe<sub>2</sub>O<sub>4</sub>. However, after 15 redox cycles, Ni-Fe carriers demonstrate a block structure due to agglomeration, causing a decrease in reactivity.<sup>184,185</sup> Therefore, nanocomposites of NiFe<sub>2</sub>O<sub>4</sub> impregnated on silica matrix were synthesized, which prevents particle aggregation due to enhanced dispersion of spinel NiFe<sub>2</sub>O<sub>4</sub>. Olhero and co-workers conducted a study to understand the effect of heat treatment on agglomeration using zinc-substituted Ni ferrite (Ni<sub>0.8</sub>Zn<sub>0.2</sub>Fe<sub>2</sub>O<sub>4</sub>) powders. Increasing the calcination temperature from 400 °C to 1200 °C causes a 776% increase in the average particle size and a 99.9% decrease in the specific surface area due to agglomeration.<sup>186</sup> Scheffe *et al.* synthesized Co<sub>0.85</sub>Fe<sub>2.15</sub>O<sub>4</sub> Fe-OC *via* atomic layer deposition on ZrO<sub>2</sub>, demonstrating stable and improved reactivity and ameliorating agglomeration.<sup>80</sup>

The commercial CL process would involve Fe-OC fluidization for thousands of hours under varying temperatures and the constant swing of oxidation states.<sup>187</sup> The continuous mechanical, thermal, and chemical stresses can lead to chipping, disintegration, abrasion, or fragmentation of the Fe-OC, broadly classified as attrition.<sup>188</sup> As illustrated in Fig. 6(d), abrasion, characterized by the chipping of uneven surfaces of the parent Fe-OC, is majorly observed at lower particle circulation rates.



Fragmentation, observed at higher Fe-OC circulation rates, leads to many sub-particles forming fragments. Attrition of Fe-OCs results in particle make-up cost, which is a function of attrition rate ( $A$ ), solid circulation rate, and cost of Fe-OC manufacture. Therefore, attrition can greatly influence the overall operating costs of the CL plant, and hence, tremendous efforts are focused on decreasing the attrition rate and increasing the Fe-OC lifetime. Adanez and co-workers found that 20 wt%  $\text{Fe}_2\text{O}_3$  supported on  $\text{Al}_2\text{O}_3$  demonstrates low  $A$  of 0.09–0.14% per h, translating into a Fe-OC lifetime of 700–1150 hours at an operating temperature of  $\sim 900$  °C.<sup>189</sup> Pans *et al.* also utilized low-cost iron ore containing 76 wt%  $\text{Fe}_2\text{O}_3$  in the CLC unit to generate syngas at 830–930 °C and observed a low  $A$  of 0.05% per h, corresponding to a lifetime of 2000 hours.<sup>190</sup> Mei *et al.* utilized four different Fe-OC compositions: 65.6%  $\text{Mn}_3\text{O}_4$ –18.6%  $\text{Fe}_2\text{O}_3$ , 67.5%  $\text{Mn}_3\text{O}_4$ –8.4%  $\text{Fe}_2\text{O}_3$ , 71.8%  $\text{Mn}_3\text{O}_4$ –6%  $\text{Fe}_2\text{O}_3$ , 80.7%  $\text{Mn}_3\text{O}_4$ –5.2%  $\text{Fe}_2\text{O}_3$ , dispersed over  $\text{Al}_2\text{O}_3$  as the inert support and observed that Fe-OC composed of 65.6%  $\text{Mn}_3\text{O}_4$  achieves the lowest  $A$  of 0.0625% per h increasing the lifetime to 1600 hours. The remaining compositions had an attrition rate in the range of 0.1–0.67% per h with an OC lifetime of 1000–150 hours.<sup>191</sup> Chung *et al.* have demonstrated stable performance of Fe-OC supported on Al-based inert for over 3000 cycles.<sup>192</sup> It can be concluded that Al-based supports have proven to be promising in enhancing the lifetime of Fe-OC. Moreover, it has been observed for most of the synthetic Fe-OCs that the crushing strength increases with an increase in calcination temperature from 950–1600 °C but leads to a loss in the reactive capability of the material. Natural ores of iron-containing mixed-metal oxides of  $\text{SiO}_2$ ,  $\text{Al}_2\text{O}_3$ ,  $\text{CaO}$ ,  $\text{Na}_2\text{O}$ ,  $\text{K}_2\text{O}$ ,  $\text{MgO}$ , and  $\text{TiO}_2$  show a positive effect on reducing the  $A$ . However, fewer research efforts have focused on natural Fe-OC due to their low reactivity.<sup>153</sup> While attrition presents a significant challenge to CL technology, the techno-economic evaluation conducted by Zhang *et al.* estimates that even with frequent solid make-up, the Fe-OC based CL process can be economically more attractive compared to the current state-of-the-art processes for commodity chemical production.<sup>50</sup>

Moreover, it is important to understand that the target application and the method of operation critically influence the choice of the active material and the Fe-OC composition. While the addition of a component may increase the attrition rate of the Fe-OC particles, it may prevent the deactivation of the Fe-OC due to carbon deposition. If the operational strategy of the process involves using fluidized beds, the addition of the component might be impractical since the process would require frequent solid makeup due to low OC lifetime. However, the Fe-OC can be well-suited for a fixed bed process where strength can be compromised to prevent carbon deposition for extended periods of operation. Similarly, increasing the strength and lowering the attrition rates may result in a compromise with the reactivity of the Fe-OC. In practice, the OC developed for larger scales of operation involves a delicate balance and an optimized trade-off of the extent to which each challenge is tackled by incorporating multiple components. Therefore, the precise compositions of most of the Fe-OCs that have been tested for a higher scale of operation are protected in the form of proprietary information.

## 5 Conclusion and perspectives

Chemical looping emerges as a highly promising technology in the pursuit of sustainable energy solutions. Metal ferrites have shown great potential as OCs for CL processes, offering a path toward reducing greenhouse gas emissions and improving the sustainability of industrial chemical production. Nevertheless, there remains a significant need to refine these materials and their associated processes to address current limitations and challenges. This review has thoroughly explored metal ferrites, highlighting their fundamental properties and critical role in advancing the efficacy of chemical looping processes. Innovation in Fe-OC is geared towards boosting OTC, increasing surface reactivity, and enhancing thermal stability. These improvements can be achieved through the development of composite metal ferrite and bimetallic systems. Employing nanoscale engineering and surface modification techniques could also markedly enhance the overall performance of Fe-OC for novel CL processes. Additionally, process optimization is vital for refining ferrite-based CL processes. This involves using sophisticated computational models and simulations to refine reactor designs and operational parameters, ensuring optimal interaction between metal ferrites and reactants and reducing energy losses. Integrating robust systems that align CL with current industrial practices could ease the adoption and implementation across various sectors. As these technologies have completed successful pilot testing and are progressing toward commercialization, enhancing lifecycle assessments to meet sustainability criteria will also be crucial. Fe-OCs-based CL processes can offer cost advantages over other transition metal oxide-based CL technologies for producing commodity chemicals. Therefore, the ongoing development of Fe-OCs and their derivative CL processes is expected to continue playing a critical role in advancing sustainable technologies, which will significantly contribute to scientific efforts and industrial practices to mitigate climate change and enhance clean energy production.

## Abbreviations

BTU	British thermal units
$\text{H}_2$	Hydrogen
$\text{CH}_3\text{OH}$	Methanol
$\text{C}_2\text{H}_5\text{OH}$	Ethanol
$\text{NH}_3$	Ammonia
ATR	Auto-thermal reforming
SMR	Steam methane reforming
CL	Chemical looping
$\text{CO}_2$	Carbon dioxide
$\text{H}_2\text{O}$	Steam
CO	Carbon monoxide
$\text{NO}_x$	Nitrous oxides ( $\text{NO}_x$ )
$\text{NiO}$	Nickel oxide
$\text{CuO}$	Copper oxide
$\text{Fe}_2\text{O}_3$	Iron oxide
$\text{Cr}_2\text{O}_3$	Chromium oxide
$\text{V}_2\text{O}_5$	Vanadium oxide

$Mn_2O_3$	Manganese oxide
$Co_3O_4$	Cobalt oxide
$CeO_2$	Ceria
OC	Oxygen carriers
Fe-OC	Ferrite-based oxygen carriers
$FeTiO_3$	Iron-titanium oxide
$CH_4$	Methane
CLC	Chemical looping combustion
CLG	Chemical looping gasification
CLPO	Chemical looping partial oxidation
CLR	Chemical looping reforming
CLHG	Chemical looping hydrogen generation;
$\Delta E_{vac}$	Vacancy formation energy
YSZ8-CS	8 mol% yttria-stabilized zirconium oxide core-shell
YSZ10-CS	10 mol% yttria-stabilized zirconium oxide core-shell
OTC	Oxygen transport capacity
OSU	Ohio State University
Na	Sodium
$MgO$	Magnesium oxide
$K_2CO_3$	Potassium carbonate
$T_{Tam}$	Tammann temperatures
$Ni_{0.8}Zn_{0.2}Fe_2O_4$	Zinc-substituted Ni ferrite
A	Attrition rate

## Data availability

No primary research results, software, or code have been included, and no new data were generated or analyzed as part of this review.

## Author contributions

Tanay A. Jawdekar and Ishani Karki Kudva contributed equally to this work and are co-first authors. Tanay A. Jawdekar: conceptualization, formal analysis, methodology, visualization, writing – original draft, writing – review & editing. Ishani Karki Kudva: conceptualization, methodology, visualization, writing – original draft, writing – review & editing. Sudeshna Gun: writing – original draft, visualization, writing – review & editing. Shekhar G. Shinde: writing – original draft, visualization, writing – review & editing. Ashin A. Sunny: writing – original draft, visualization, writing – review & editing. Zhuo Cheng: supervision, writing – original draft, writing – review & editing. Liang-Shih Fan: resources, supervision, writing – review & editing.

## Conflicts of interest

The authors declare that they have no known competing financial interests or personal relationships that could have influenced this study.

## Acknowledgements

The authors greatly appreciate the helpful discussions with Dr Sonu Kumar, Dr Rushikesh K. Joshi, and Dr Anuj Joshi. Their

guidance and support were extremely valuable in shaping the manuscript and improving the quality of this work.

## References

- 1 A. Joshi, V. Shah, P. Mohapatra, S. Kumar, R. K. Joshi, M. Kathe, L. Qin, A. Tong and L.-S. Fan, Chemical Looping-A Perspective on the next-Gen Technology for Efficient Fossil Fuel Utilization, *Adv. Appl. Energy*, 2021, **3**, 100044, DOI: [10.1016/j.adapen.2021.100044](https://doi.org/10.1016/j.adapen.2021.100044).
- 2 U.S. Energy Information Administration (EIA), Narrative, <https://www.eia.gov/outlooks/aoe/narrative/index.php>, accessed 2024-08-28.
- 3 U.S. Energy Information Administration (EIA), Use of energy in industry, <https://www.eia.gov/energyexplained/use-of-energy/industry.php>, accessed 2024-08-28.
- 4 MarketsandMarkets, Syngas Market Size, Industry Share Forecast Trends Report, <https://www.marketsandmarkets.com/Market-Reports/syngas-market-1178.html>, accessed 2024-08-28.
- 5 S. Abuelgasim, W. Wang and A. Abdalazeez, A Brief Review for Chemical Looping Combustion as a Promising  $CO_2$  Capture Technology: Fundamentals and Progress, *Sci. Total Environ.*, 2021, **764**, 142892, DOI: [10.1016/j.scitotenv.2020.142892](https://doi.org/10.1016/j.scitotenv.2020.142892).
- 6 A. Joshi, P. Mohapatra, R. Joshi, S. Kumar, A. Sunny, Z. Cheng, L. Qin and L.-S. Fan, Advances in Chemical Looping Combustion Technology, in *Combustion Chemistry and the Carbon Neutral Future*, Elsevier, 2023, pp. 383–416, DOI: [10.1016/B978-0-323-99213-8.00003-5](https://doi.org/10.1016/B978-0-323-99213-8.00003-5).
- 7 V. Shah, K. Jangam, A. Joshi, P. Mohapatra, E. Falascino and L. Fan, The Role of Chemical Looping in Industrial Gas Separation, in *Sustainable Separation Engineering*, ed. Szekely, G. and Zhao, D., Wiley, 2022, pp. 199–237, DOI: [10.1002/9781119740117.ch5](https://doi.org/10.1002/9781119740117.ch5).
- 8 S. Kumar, P. Mohapatra, R. K. Joshi, M. Warburton and L.-S. Fan, Synergistic Chemical Looping Process Coupling Natural Gas Conversion and  $NO_x$  Purification, *Energy Fuels*, 2023, **37**(10), 7268–7279, DOI: [10.1021/acs.energyfuels.3c00254](https://doi.org/10.1021/acs.energyfuels.3c00254).
- 9 P. Mohapatra, S. Kumar, A. Sunny, M. Marx, Y. Khalifa, A. H. Trout and L.-S. Fan, Natural Gas-Assisted  $NO_x$  Abatement Using Chemical Looping Scheme, *Energy Fuels*, 2024, **38**(17), 16570–16579, DOI: [10.1021/acs.energyfuels.4c01843](https://doi.org/10.1021/acs.energyfuels.4c01843).
- 10 X. Zhu, Q. Imtiaz, F. Donat, C. R. Müller and F. Li, Chemical Looping beyond Combustion – a Perspective, *Energy Environ. Sci.*, 2020, **13**(3), 772–804, DOI: [10.1039/C9EE03793D](https://doi.org/10.1039/C9EE03793D).
- 11 Q. Zhang, T. Jawdekar, S. Gun and L.-S. Fan, A Novel 2-Reactor Chemical Looping System for Hydrogen Production with Biogas as the Feedstock: Process Simulation and Comparison with Conventional Reforming Processes, *Ind. Eng. Chem. Res.*, 2024, **63**(9), 4004–4017, DOI: [10.1021/acs.iecr.3c02871](https://doi.org/10.1021/acs.iecr.3c02871).
- 12 A. Joshi, R. K. Joshi, E. Falascino, T. A. Jawdekar, S. G. Shinde, D. Baser, S. Patil and L.-S. Fan,



Thermodynamic Evaluation of the Cross-Current Moving-Bed Chemical Looping Configuration for Efficient Conversion of Biomass to Syngas, *Energy Fuels*, 2023, 37(21), 16744–16756, DOI: [10.1021/acs.energyfuels.3c02934](https://doi.org/10.1021/acs.energyfuels.3c02934).

13 K. V. Jangam, A. S. Joshi, Y.-Y. Chen, S. Mahalingam, A. A. Sunny and L.-S. Fan, Synergistic Decomposition of  $\text{H}_2\text{S}$  into  $\text{H}_2$  by  $\text{Ni}_3\text{S}_2$  over  $\text{ZrO}_2$  Support via a Sulfur Looping Scheme with  $\text{CO}_2$  Enabled Carrier Regeneration, *Chem. Eng. J.*, 2021, 426, 131815, DOI: [10.1016/j.cej.2021.131815](https://doi.org/10.1016/j.cej.2021.131815).

14 S. Kumar, T. A. Jawdekar, Z. Cheng, F. Akulwar, J. Hu, A. H. Trout and L.-S. Fan, Enhanced Decomposition of  $\text{H}_2\text{S}$  to  $\text{H}_2$  via Iron Sulfide Nanoparticles: A Comprehensive Experimental and Theoretical Evaluation, *Chem. Eng. J.*, 2024, 499, 156117, DOI: [10.1016/j.cej.2024.156117](https://doi.org/10.1016/j.cej.2024.156117).

15 M. Luo, Y. Yi, S. Wang, Z. Wang, M. Du, J. Pan and Q. Wang, Review of Hydrogen Production Using Chemical-Looping Technology, *Renewable Sustainable Energy Rev.*, 2018, 81, 3186–3214, DOI: [10.1016/j.rser.2017.07.007](https://doi.org/10.1016/j.rser.2017.07.007).

16 A. Joshi, S. Kumar, M. Marx, A. H. Trout, S. Gun, Z. Mohammad, Y. Khalifa and L.-S. Fan, Chemical Looping Methanol Oxidation Using Supported Vanadium Phosphorous Oxide Carriers for Formaldehyde Production, *J. Mater. Chem. A*, 2024, 12(13), 7680–7692, DOI: [10.1039/D3TA07468D](https://doi.org/10.1039/D3TA07468D).

17 J. Adámez and A. Abad, Chemical-Looping Combustion: Status and Research Needs, *Proc. Combust. Inst.*, 2019, 37(4), 4303–4317, DOI: [10.1016/j.proci.2018.09.002](https://doi.org/10.1016/j.proci.2018.09.002).

18 A. A. Sunny, Q. Meng, S. Kumar, R. Joshi and L.-S. Fan, Nanoscaled Oxygen Carrier-Driven Chemical Looping for Carbon Neutrality: Opportunities and Challenges, *Acc. Chem. Res.*, 2023, 56(23), 3404–3416, DOI: [10.1021/acs.accounts.3c00517](https://doi.org/10.1021/acs.accounts.3c00517).

19 D. Zeng, Y. Qiu, S. Peng, C. Chen, J. Zeng, S. Zhang and R. Xiao, Enhanced Hydrogen Production Performance through Controllable Redox Exsolution within  $\text{CoFeAlO}_x$  Spinel Oxygen Carrier Materials, *J. Mater. Chem. A*, 2018, 6(24), 11306–11316, DOI: [10.1039/C8TA02477D](https://doi.org/10.1039/C8TA02477D).

20 S. Kumar, Z. Cheng, S. Gun, L. Qin, H. Colijn, Z. Mohammad and L.-S. Fan, Nanoscale Structural Transformations in  $\text{LaFeO}_3$  Oxygen Carriers for Enhanced Reactivity in Chemical Looping Combustion, *Powder Technol.*, 2024, 444, 119988, DOI: [10.1016/j.powtec.2024.119988](https://doi.org/10.1016/j.powtec.2024.119988).

21 X. Hua and W. Wang, Chemical Looping Combustion: A New Low-Dioxin Energy Conversion Technology, *J. Environ. Sci.*, 2015, 32, 135–145, DOI: [10.1016/j.jes.2014.09.044](https://doi.org/10.1016/j.jes.2014.09.044).

22 T. Song, L. Shen, J. Xiao, D. Chen, H. Gu and S. Zhang, Nitrogen Transfer of Fuel-N in Chemical Looping Combustion, *Combust. Flame*, 2012, 159(3), 1286–1295, DOI: [10.1016/j.combustflame.2011.10.024](https://doi.org/10.1016/j.combustflame.2011.10.024).

23 L. Zeng, Z. Cheng, J. A. Fan, L.-S. Fan and J. Gong, Metal Oxide Redox Chemistry for Chemical Looping Processes, *Nat. Rev. Chem.*, 2018, 2(11), 349–364, DOI: [10.1038/s41570-018-0046-2](https://doi.org/10.1038/s41570-018-0046-2).

24 C. H. Lin, C. Wan, Z. Ru, C. Cremers, P. Mohapatra, D. L. Mantle, K. Tamakuwala, A. B. Höfelmann, M. W. Kanan, J. Rivas-Davila and J. A. Fan, Electrified Thermochemical Reaction Systems with High-Frequency Metamaterial Reactors, *Joule*, 2024, 8(10), 2938–2949, DOI: [10.1016/j.joule.2024.07.017](https://doi.org/10.1016/j.joule.2024.07.017).

25 A. Lyngfelt, Chemical Looping Combustion: Status and Development Challenges, *Energy Fuels*, 2020, 34(8), 9077–9093, DOI: [10.1021/acs.energyfuels.0c01454](https://doi.org/10.1021/acs.energyfuels.0c01454).

26 Y. Zhu, X. Liu, S. Jin, H. Chen, W. Lee, M. Liu and Y. Chen, Anionic Defect Engineering of Transition Metal Oxides for Oxygen Reduction and Evolution Reactions, *J. Mater. Chem. A*, 2019, 7(11), 5875–5897, DOI: [10.1039/C8TA12477A](https://doi.org/10.1039/C8TA12477A).

27 L.-S. Fan, *Chemical Looping Partial Oxidation: Gasification, Reforming, and Chemical Syntheses*, Cambridge University Press, Cambridge, 1st edn, 2017.

28 L.-S. Fan, *Chemical Looping Systems for Fossil Energy Conversions*, Wiley-AIChE, Hoboken, NJ, 2010.

29 T. Mattisson, M. Johansson and A. Lyngfelt, The Use of  $\text{NiO}$  as an Oxygen Carrier in Chemical-Looping Combustion, *Fuel*, 2006, 85(5–6), 736–747, DOI: [10.1016/j.fuel.2005.07.021](https://doi.org/10.1016/j.fuel.2005.07.021).

30 C. R. Forero, P. Gayán, F. García-Labiano, L. F. de Diego, A. Abad and J. Adámez, High Temperature Behaviour of a  $\text{CuO}/\gamma\text{-Al}_2\text{O}_3$  Oxygen Carrier for Chemical-Looping Combustion, *Int. J. Greenhouse Gas Control*, 2011, 5(4), 659–667, DOI: [10.1016/j.ijgge.2011.03.005](https://doi.org/10.1016/j.ijgge.2011.03.005).

31 R. Bhosale, F. AlMomani and G. Takalkar, Thermodynamic Analysis of Solar-Driven Chemical Looping Steam Methane Reforming over  $\text{Cr}_2\text{O}_3/\text{Cr}$  Redox Pair, *Int. J. Hydrogen Energy*, 2020, 45(17), 10370–10380, DOI: [10.1016/j.ijhydene.2019.08.205](https://doi.org/10.1016/j.ijhydene.2019.08.205).

32 J. Cao, S. Ma and T. Song,  $\text{V}_2\text{O}_5/\text{TiO}_2$  Acting as Both Oxygen Carrier and Catalyst for Chemical Looping Oxidation of  $\text{H}_2\text{S}$  at a Low Temperature, *Fuel*, 2022, 320, 123999, DOI: [10.1016/j.fuel.2022.123999](https://doi.org/10.1016/j.fuel.2022.123999).

33 Y. Cao, B. He, W. Tong, H. Yao and Z. Duan, On the Kinetics of  $\text{Mn}_2\text{O}_3/\text{ZrO}_2$  Oxygen Carrier for Chemical Looping Air Separation, *Chem. Eng. Process.*, 2019, 136, 82–91, DOI: [10.1016/j.cep.2019.01.001](https://doi.org/10.1016/j.cep.2019.01.001).

34 H. A. Alalwan, D. M. Cwiertny and V. H. Grassian,  $\text{Co}_3\text{O}_4$  Nanoparticles as Oxygen Carriers for Chemical Looping Combustion: A Materials Characterization Approach to Understanding Oxygen Carrier Performance, *Chem. Eng. J.*, 2017, 319, 279–287, DOI: [10.1016/j.cej.2017.02.134](https://doi.org/10.1016/j.cej.2017.02.134).

35 Y. Zheng, X. Zhu, H. Wang, K. Li, Y. Wang and Y. Wei, Characteristic of Macroporous  $\text{CeO}_2\text{-ZrO}_2$  Oxygen Carrier for Chemical-Looping Steam Methane Reforming, *J. Rare Earths*, 2014, 32(9), 842–848, DOI: [10.1016/S1002-0721\(14\)60151-4](https://doi.org/10.1016/S1002-0721(14)60151-4).

36 E. R. Monazam, R. W. Breault, R. Siriwardane, G. Richards and S. Carpenter, Kinetics of the Reduction of Hematite ( $\text{Fe}_2\text{O}_3$ ) by Methane ( $\text{CH}_4$ ) during Chemical Looping



Combustion: A Global Mechanism, *Chem. Eng. J.*, 2013, **232**, 478–487, DOI: [10.1016/j.cej.2013.07.091](https://doi.org/10.1016/j.cej.2013.07.091).

37 E. R. Monazam, R. W. Breault, R. Siriwardane and D. D. Miller, Thermogravimetric Analysis of Modified Hematite by Methane ( $\text{CH}_4$ ) for Chemical-Looping Combustion: A Global Kinetics Mechanism, *Ind. Eng. Chem. Res.*, 2013, **52**(42), 14808–14816, DOI: [10.1021/ie4024116](https://doi.org/10.1021/ie4024116).

38 L.-S. Fan, F. Kong and V. Shah, Chemical Looping Systems with at Least Two Particle Types, US20230113165A1, April 13, 2023, <https://patents.google.com/patent/US20230113165A1/en>.

39 M. J. den Exter, W. G. Haije and J. F. Vente, Viability of ITM Technology for Oxygen Production and Oxidation Processes: Material, System, and Process Aspects, in *Inorganic Membranes for Energy and Environmental Applications*, ed. Bose, A. C., Springer New York, New York, NY, 2009, pp. 27–51, DOI: [10.1007/978-0-387-34526-0\\_2](https://doi.org/10.1007/978-0-387-34526-0_2).

40 D. N. Haerani, C. N. Ulan, Y. Sarwanto, A. Mulyawan, I. G. A. P. Adnyana, E. Sukirman, Yunasfi and W. A. Adi, Pseudobrookite  $\text{Fe}_{2-2x}\text{Co}_x\text{Ti}_{1-\frac{1}{2}x}\text{O}_5$ : Structural, Magnetic Phase Transformation and Reflection Loss Characteristic, *Materialia*, 2023, **27**, 101692, DOI: [10.1016/j.mtla.2023.101692](https://doi.org/10.1016/j.mtla.2023.101692).

41 N. Tarasova, Layered Perovskites  $\text{BaLn}_n\text{In}_n\text{O}_{3n+1}$  ( $n = 1, 2$ ) for Electrochemical Applications: A Mini Review, *Membranes*, 2022, **13**(1), 34, DOI: [10.3390/membranes13010034](https://doi.org/10.3390/membranes13010034).

42 G. Pilania, V. Kocevski, J. A. Valdez, C. R. Kreller and B. P. Uberuaga, Prediction of Structure and Cation Ordering in an Ordered Normal-Inverse Double Spinel, *Commun. Mater.*, 2020, **1**(1), 84, DOI: [10.1038/s43246-020-00082-2](https://doi.org/10.1038/s43246-020-00082-2).

43 E. Falascino, R. K. Joshi, S. Kumar, T. Jawdekar, I. K. Kudva, S. G. Shinde, Z. Cheng, A. Tong and L.-S. Fan, Enabling Plastic Waste Gasification by Autothermal Chemical Looping with > 90% Syngas Purity for Versatile Feedstock Handling, *Appl. Energy Combust. Sci.*, 2024, **19**, 100270, DOI: [10.1016/j.jaecs.2024.100270](https://doi.org/10.1016/j.jaecs.2024.100270).

44 C. Park, R. K. Joshi, E. Falascino, Y. Pottimurthy, D. Xu, D. Wang, A. Sunny, S. Hwang, A. S. Joshi, P. Mohapatra, S. Kumar, Q. Zhang, Q. Meng, V. Shah, A. Tong and L.-S. Fan, Biomass Gasification: Sub-Pilot Operation of >600 h with Extensive Tar Cracking Property and High Purity Syngas Production at  $\text{H}_2:\text{CO}$  Ratio ~2 Using Moving Bed Redox Looping Technology, *Fuel Process. Technol.*, 2023, **252**, 107966, DOI: [10.1016/j.fuproc.2023.107966](https://doi.org/10.1016/j.fuproc.2023.107966).

45 S. Luo, L. Zeng, D. Xu, M. Kathe, E. Chung, N. Deshpande, L. Qin, A. Majumder, T.-L. Hsieh, A. Tong, Z. Sun and L.-S. Fan, Shale Gas-to-Syngas Chemical Looping Process for Stable Shale Gas Conversion to High Purity Syngas with a  $\text{H}_2:\text{CO}$  Ratio of 2: 1, *Energy Environ. Sci.*, 2014, **7**(12), 4104–4117, DOI: [10.1039/C4EE02892A](https://doi.org/10.1039/C4EE02892A).

46 T.-L. Hsieh, D. Xu, Y. Zhang, S. Nadgouda, D. Wang, C. Chung, Y. Pottimurthy, M. Guo, Y.-Y. Chen, M. Xu, P. He, L.-S. Fan and A. Tong, 250 KW<sub>th</sub> High Pressure Pilot Demonstration of the Syngas Chemical Looping System for High Purity H<sub>2</sub> Production with CO<sub>2</sub> Capture, *Appl. Energy*, 2018, **230**, 1660–1672, DOI: [10.1016/j.apenergy.2018.09.104](https://doi.org/10.1016/j.apenergy.2018.09.104).

47 D. Xu, Y. Zhang, T.-L. Hsieh, M. Guo, L. Qin, C. Chung, L.-S. Fan and A. Tong, A Novel Chemical Looping Partial Oxidation Process for Thermochemical Conversion of Biomass to Syngas, *Appl. Energy*, 2018, **222**, 119–131, DOI: [10.1016/j.apenergy.2018.03.130](https://doi.org/10.1016/j.apenergy.2018.03.130).

48 Y. Zhang, D. Wang, Y. Pottimurthy, F. Kong, T.-L. Hsieh, B. Sakadjian, C. Chung, C. Park, D. Xu, J. Bao, L. Velazquez-Vargas, M. Guo, P. Sandvik, S. Nadgouda, T. J. Flynn, A. Tong and L.-S. Fan, Coal Direct Chemical Looping Process: 250 kW Pilot-Scale Testing for Power Generation and Carbon Capture, *Appl. Energy*, 2021, **282**, 116065, DOI: [10.1016/j.apenergy.2020.116065](https://doi.org/10.1016/j.apenergy.2020.116065).

49 Q. Zhang, R. K. Joshi, D. Xu, A. Tong and L.-S. Fan, A Novel Moving Bed Chemical Looping Process with Integration of Combustor Heat Exchangers for Hydrogen Production: Process Simulation and Techno-Economic Analysis, *Int. J. Hydrogen Energy*, 2024, **49**, 823–839, DOI: [10.1016/j.ijhydene.2023.07.300](https://doi.org/10.1016/j.ijhydene.2023.07.300).

50 Q. Zhang, A. Tong and L.-S. Fan, Hydrogen and Electric Power Cogeneration in Novel Redox Chemical Looping Systems: Operational Schemes and Tech-Economic Impact, *Ind. Eng. Chem. Res.*, 2023, **62**(12), 5065–5082, DOI: [10.1021/acs.iecr.2c03834](https://doi.org/10.1021/acs.iecr.2c03834).

51 C. Park, T.-L. Hsieh, Y. Pottimurthy, V. Shah, D. Xu, Y.-Y. Chen, L.-S. Fan and A. Tong, Design and Operations of a 15 kW<sub>th</sub> Subpilot Unit for the Methane-to-Syngas Chemical Looping Process with CO<sub>2</sub> Utilization, *Ind. Eng. Chem. Res.*, 2020, **59**(15), 6886–6899, DOI: [10.1021/acs.iecr.9b05577](https://doi.org/10.1021/acs.iecr.9b05577).

52 X. Zhu, K. Li, Y. Wei, H. Wang and L. Sun, Chemical-Looping Steam Methane Reforming over a CeO<sub>2</sub>–Fe<sub>2</sub>O<sub>3</sub> Oxygen Carrier: Evolution of Its Structure and Reducibility, *Energy Fuels*, 2014, **28**(2), 754–760, DOI: [10.1021/ef402203a](https://doi.org/10.1021/ef402203a).

53 Z. Huang, F. He, D. Chen, K. Zhao, G. Wei, A. Zheng, Z. Zhao and H. Li, Investigation on Reactivity of Iron Nickel Oxides in Chemical Looping Dry Reforming, *Energy*, 2016, **116**, 53–63, DOI: [10.1016/j.energy.2016.09.101](https://doi.org/10.1016/j.energy.2016.09.101).

54 I. K. Kudva, S. G. Shinde, R. K. Joshi, T. A. Jawdekar, S. Gun, S. Kumar, A. A. Sunny, D. Kulchytsky, Z. Cheng and L.-S. Fan, Low Carbon Formaldehyde Generation from Chemical Looping Gasification of Heterogeneous Solid Waste, *Energy Fuels*, 2024, **38**(21), 20839–20850, DOI: [10.1021/acs.energyfuels.4c02643](https://doi.org/10.1021/acs.energyfuels.4c02643).

55 L.-S. Fan, S. Kumar, A. A. Sunny, R. K. Joshi, P. Mohapatra, A. S. Joshi and Q. Marashdeh, Multiphase Entrepreneurship: An Academic Reflection, *Powder Technol.*, 2024, **439**, 119654, DOI: [10.1016/j.powtec.2024.119654](https://doi.org/10.1016/j.powtec.2024.119654).

56 F. Li, Z. Sun, S. Luo and L.-S. Fan, Ionic Diffusion in the Oxidation of Iron—Effect of Support and Its Implications



to Chemical Looping Applications, *Energy Environ. Sci.*, 2011, **4**(3), 876, DOI: [10.1039/c0ee00589d](https://doi.org/10.1039/c0ee00589d).

57 Z. Cheng, L. Qin, J. A. Fan and L.-S. Fan, New Insight into the Development of Oxygen Carrier Materials for Chemical Looping Systems, *Engineering*, 2018, **4**(3), 343–351, DOI: [10.1016/j.eng.2018.05.002](https://doi.org/10.1016/j.eng.2018.05.002).

58 L. Qin, A. Majumder, J. A. Fan, D. Kopechek and L.-S. Fan, Evolution of Nanoscale Morphology in Single and Binary Metal Oxide Microparticles during Reduction and Oxidation Processes, *J. Mater. Chem. A*, 2014, **2**(41), 17511–17520, DOI: [10.1039/C4TA04338C](https://doi.org/10.1039/C4TA04338C).

59 L. Qin, Z. Cheng, J. A. Fan, D. Kopechek, D. Xu, N. Deshpande and L.-S. Fan, Nanostructure Formation Mechanism and Ion Diffusion in Iron–Titanium Composite Materials with Chemical Looping Redox Reactions, *J. Mater. Chem. A*, 2015, **3**(21), 11302–11312, DOI: [10.1039/C5TA01853F](https://doi.org/10.1039/C5TA01853F).

60 Z. Cheng, L. Qin, M. Guo, J. A. Fan, D. Xu and L.-S. Fan, Methane Adsorption and Dissociation on Iron Oxide Oxygen Carriers: The Role of Oxygen Vacancies, *Phys. Chem. Chem. Phys.*, 2016, **18**(24), 16423–16435, DOI: [10.1039/C6CP01287F](https://doi.org/10.1039/C6CP01287F).

61 V. Shah, Z. Cheng, P. Mohapatra and L.-S. Fan, Enhanced Methane Conversion Using Ni-Doped Calcium Ferrite Oxygen Carriers in Chemical Looping Partial Oxidation Systems with CO<sub>2</sub> Utilization, *React. Chem. Eng.*, 2021, **6**(10), 1928–1939, DOI: [10.1039/D1RE00150G](https://doi.org/10.1039/D1RE00150G).

62 M. Guo, Z. Cheng, Y. Liu, L. Qin, J. Goetze, J. A. Fan and L.-S. Fan, Cobalt Doping Modification for Enhanced Methane Conversion at Low Temperature in Chemical Looping Reforming Systems, *Catal. Today*, 2020, **350**, 156–164, DOI: [10.1016/j.cattod.2019.06.016](https://doi.org/10.1016/j.cattod.2019.06.016).

63 L. Qin, M. Guo, Y. Liu, Z. Cheng, J. A. Fan and L.-S. Fan, Enhanced Methane Conversion in Chemical Looping Partial Oxidation Systems Using a Copper Doping Modification, *Appl. Catal., B*, 2018, **235**, 143–149, DOI: [10.1016/j.apcatb.2018.04.072](https://doi.org/10.1016/j.apcatb.2018.04.072).

64 Y. Guan, G. Zhang, R. Wang, Y. Wang and Y. Liu, Study on the Synergistic Effect and Oxygen Vacancy of CeO<sub>2</sub>/Fe<sub>2</sub>O<sub>3</sub> Oxygen Carrier for Improving Reactivity in Carbon Monoxide Chemical Looping Combustion, *Fuel*, 2024, **357**, 129832, DOI: [10.1016/j.fuel.2023.129832](https://doi.org/10.1016/j.fuel.2023.129832).

65 A. Shafiefarhood, N. Galinsky, Y. Huang, Y. Chen and F. Li, Fe<sub>2</sub>O<sub>3</sub>@La<sub>x</sub>Sr<sub>1-x</sub>FeO<sub>3</sub> Core–Shell Redox Catalyst for Methane Partial Oxidation, *ChemCatChem*, 2014, **6**(3), 790–799, DOI: [10.1002/cctc.201301104](https://doi.org/10.1002/cctc.201301104).

66 L. Neal, A. Shafiefarhood and F. Li, Effect of Core and Shell Compositions on MeOx@La<sub>y</sub>Sr<sub>1-y</sub>FeO<sub>3</sub> Core–Shell Redox Catalysts for Chemical Looping Reforming of Methane, *Appl. Energy*, 2015, **157**, 391–398, DOI: [10.1016/j.apenergy.2015.06.028](https://doi.org/10.1016/j.apenergy.2015.06.028).

67 N. L. Galinsky, A. Shafiefarhood, Y. Chen, L. Neal and F. Li, Effect of Support on Redox Stability of Iron Oxide for Chemical Looping Conversion of Methane, *Appl. Catal., B*, 2015, **164**, 371–379, DOI: [10.1016/j.apcatb.2014.09.023](https://doi.org/10.1016/j.apcatb.2014.09.023).

68 S. Ma, S. Chen, M. Zhu, Z. Zhao, J. Hu, M. Wu, S. Toan and W. Xiang, Enhanced Sintering Resistance of Fe<sub>2</sub>O<sub>3</sub>/CeO<sub>2</sub> Oxygen Carrier for Chemical Looping Hydrogen Generation Using Core–Shell Structure, *Int. J. Hydrogen Energy*, 2019, **44**(13), 6491–6504, DOI: [10.1016/j.ijhydene.2019.01.167](https://doi.org/10.1016/j.ijhydene.2019.01.167).

69 F. Blaschke, M. Bele, Š. Polak, B. Bitschnau and V. Hacker, Core–Shell Iron-Based Oxygen Carrier Material for Highly Efficient Green Hydrogen Production by Chemical Looping, *Mater. Today*, 2024, **75**, 37–56, DOI: [10.1016/j.mattod.2024.03.016](https://doi.org/10.1016/j.mattod.2024.03.016).

70 X. Yin, S. Wang, R. Sun, S. Jiang and L. Shen, A Ce–Fe Oxygen Carrier with a Core–Shell Structure for Chemical Looping Steam Methane Reforming, *Ind. Eng. Chem. Res.*, 2020, **59**(21), 9775–9786, DOI: [10.1021/acs.iecr.0c00055](https://doi.org/10.1021/acs.iecr.0c00055).

71 V. Shah, P. Mohapatra and L.-S. Fan, Thermodynamic and Process Analyses of Syngas Production Using Chemical Looping Reforming Assisted by Flexible Dicalcium Ferrite-Based Oxygen Carrier Regeneration, *Energy Fuels*, 2020, **34**(5), 6490–6500, DOI: [10.1021/acs.energyfuels.0c00479](https://doi.org/10.1021/acs.energyfuels.0c00479).

72 X. Wang, Z. Chen, M. Hu, Y. Tian, X. Jin, S. Ma, T. Xu, Z. Hu, S. Liu, D. Guo and B. Xiao, Chemical Looping Combustion of Biomass Using Metal Ferrites as Oxygen Carriers, *Chem. Eng. J.*, 2017, **312**, 252–262, DOI: [10.1016/j.cej.2016.11.143](https://doi.org/10.1016/j.cej.2016.11.143).

73 Y. Fan, R. Siriwardane and H. Tian, Trimetallic Oxygen Carriers CuFeMnO<sub>4</sub>, CuFeMn<sub>2</sub>O<sub>4</sub>, and CuFe<sub>0.5</sub>Mn<sub>1.5</sub>O<sub>4</sub> for Chemical Looping Combustion, *Energy Fuels*, 2015, **29**(10), 6616–6624, DOI: [10.1021/acs.energyfuels.5b01388](https://doi.org/10.1021/acs.energyfuels.5b01388).

74 W. Benincosa, R. Siriwardane, H. Tian and J. Riley, Unique Phase Identification of Trimetallic Copper Iron Manganese Oxygen Carrier Using Simultaneous Differential Scanning Calorimetry/Thermogravimetric Analysis during Chemical Looping Combustion Reactions with Methane, *Appl. Energy*, 2017, **203**, 522–534, DOI: [10.1016/j.apenergy.2017.06.061](https://doi.org/10.1016/j.apenergy.2017.06.061).

75 Z. Huang, A. Zheng, Z. Deng, G. Wei, K. Zhao, D. Chen, F. He, Z. Zhao, H. Li and F. Li, In-Situ Removal of Toluene as a Biomass Tar Model Compound Using NiFe<sub>2</sub>O<sub>4</sub> for Application in Chemical Looping Gasification Oxygen Carrier, *Energy*, 2020, **190**, 116360, DOI: [10.1016/j.energy.2019.116360](https://doi.org/10.1016/j.energy.2019.116360).

76 V. Shah, Z. Cheng, D. S. Baser, J. A. Fan and L.-S. Fan, Highly Selective Production of Syngas from Chemical Looping Reforming of Methane with CO<sub>2</sub> Utilization on MgO-Supported Calcium Ferrite Redox Materials, *Appl. Energy*, 2021, **282**, 116111, DOI: [10.1016/j.apenergy.2020.116111](https://doi.org/10.1016/j.apenergy.2020.116111).

77 D. A. Ryzhov, I. V. Shamsutov, M. V. Patrakeev, M. A. Zavyalov and O. V. Merkulov, Self-Supported Oxygen Carrier SrFe<sub>12</sub>O<sub>19</sub> for Chemical Looping: Thermodynamic Analysis, Kinetics and Redox Stability, *Solid State Sci.*, 2024, **149**, 107471, DOI: [10.1016/j.solidstatesciences.2024.107471](https://doi.org/10.1016/j.solidstatesciences.2024.107471).

78 C. Hernández-Fontes, J. A. Mendoza-Nieto, H. A. Lara-García and H. Pfeiffer, Pentolithium Ferrite (Li<sub>5</sub>FeO<sub>4</sub>) as Highly Active Material for Hydrogen Production in the Chemical Looping Partial Oxidation of Methane, *Top. Catal.*, 2019, **62**(12–16), 884–893, DOI: [10.1007/s11244-019-01175-0](https://doi.org/10.1007/s11244-019-01175-0).



79 M. Ismail, W. Liu, M. T. Dunstan and S. A. Scott, Development and Performance of Iron Based Oxygen Carriers Containing Calcium Ferrites for Chemical Looping Combustion and Production of Hydrogen, *Int. J. Hydrogen Energy*, 2016, **41**(7), 4073–4084, DOI: [10.1016/j.ijhydene.2015.11.066](https://doi.org/10.1016/j.ijhydene.2015.11.066).

80 J. R. Scheffe, M. D. Allendorf, E. N. Coker, B. W. Jacobs, A. H. McDaniel and A. W. Weimer, Hydrogen Production via Chemical Looping Redox Cycles Using Atomic Layer Deposition-Synthesized Iron Oxide and Cobalt Ferrites, *Chem. Mater.*, 2011, **23**(8), 2030–2038, DOI: [10.1021/cm103622e](https://doi.org/10.1021/cm103622e).

81 E. Marek, W. Hu, M. Gaultois, C. P. Grey and S. A. Scott, The Use of Strontium Ferrite in Chemical Looping Systems, *Appl. Energy*, 2018, **223**, 369–382, DOI: [10.1016/j.apenergy.2018.04.090](https://doi.org/10.1016/j.apenergy.2018.04.090).

82 M. Liu, H. Wu, H. Wang, T. Chen, Z. Wang, J. Zhang, Z. Zhao and J. Wu, Enhancing Redox Stability through Metal Substitution in Nickel Ferrite for Chemical Looping Hydrogen Production via Water Splitting, *Int. J. Hydrogen Energy*, 2024, **73**, 221–230, DOI: [10.1016/j.ijhydene.2024.06.017](https://doi.org/10.1016/j.ijhydene.2024.06.017).

83 M. Abián, A. Abad, M. T. Izquierdo, P. Gayán, L. F. de Diego, F. García-Labiano and J. Adámez, Titanium Substituted Manganese-Ferrite as an Oxygen Carrier with Permanent Magnetic Properties for Chemical Looping Combustion of Solid Fuels, *Fuel*, 2017, **195**, 38–48, DOI: [10.1016/j.fuel.2017.01.030](https://doi.org/10.1016/j.fuel.2017.01.030).

84 R. Lysowski and E. Ksepko,  $\text{Cu}_x\text{Mg}_{1-x}\text{Fe}_2\text{O}_4$ -Type Spinels as Potential Oxygen Carriers for Waste Wooden Biomass Combustion, *Waste Manage.*, 2024, **175**, 146–156, DOI: [10.1016/j.wasman.2023.12.057](https://doi.org/10.1016/j.wasman.2023.12.057).

85 K. Y. Kwong, A. R. P. Harrison, J. C. Gebers, J. S. Dennis and E. J. Marek, Chemical Looping Combustion of a Biomass Char in  $\text{Fe}_2\text{O}_3$ -,  $\text{CuO}$ -, and  $\text{SrFeO}_{3-\delta}$ -Based Oxygen Carriers, *Energy Fuels*, 2022, **36**(17), 9437–9449, DOI: [10.1021/acs.energyfuels.2c01269](https://doi.org/10.1021/acs.energyfuels.2c01269).

86 Y. Kim, H. S. Lim, M. Lee, M. Kim, D. Kang and J. W. Lee, Enhanced Morphological Preservation and Redox Activity in Al-Incorporated  $\text{NiFe}_2\text{O}_4$  for Chemical Looping Hydrogen Production, *ACS Sustain. Chem. Eng.*, 2021, **9**(44), 14800–14810, DOI: [10.1021/acssuschemeng.1c04619](https://doi.org/10.1021/acssuschemeng.1c04619).

87 Z. Di, D. Yilmaz, A. Biswas, F. Cheng and H. Leion, Spinel Ferrite-Contained Industrial Materials as Oxygen Carriers in Chemical Looping Combustion, *Appl. Energy*, 2022, **307**, 118298, DOI: [10.1016/j.apenergy.2021.118298](https://doi.org/10.1016/j.apenergy.2021.118298).

88 M. Nazari, N. Ghasemi, M. M. Khan, M. Rokni and S. R. Taghavi,  $\text{Cu}_x\text{Mn}_{1-x}\text{Fe}_2\text{O}_4$  as Oxygen Carrier for Chemical Looping Steam Methane Reforming, *Chem. Phys. Impact.*, 2023, **6**, 100191, DOI: [10.1016/j.chphi.2023.100191](https://doi.org/10.1016/j.chphi.2023.100191).

89 Y. Qiu, L. Ma, M. Li, D. Cui, S. Zhang, D. Zeng and R. Xiao, Copper and Cobalt Co-Doped Ferrites as Effective Agents for Chemical Looping  $\text{CO}_2$  Splitting, *Chem. Eng. J.*, 2020, **387**, 124150, DOI: [10.1016/j.cej.2020.124150](https://doi.org/10.1016/j.cej.2020.124150).

90 M. Lee, Y. Kim, H. S. Lim, A. Jo, D. Kang and J. W. Lee, Reverse Water–Gas Shift Chemical Looping Using a Core–Shell Structured Perovskite Oxygen Carrier, *Energies*, 2020, **13**(20), 5324, DOI: [10.3390/en13205324](https://doi.org/10.3390/en13205324).

91 M. Rydén, A. Lyngfelt, T. Mattisson, D. Chen, A. Holmen and E. Bjørgum, Novel Oxygen-Carrier Materials for Chemical-Looping Combustion and Chemical-Looping Reforming;  $\text{La}_x\text{Sr}_{1-x}\text{Fe}_y\text{Co}_{1-y}\text{O}_{3-\delta}$  Perovskites and Mixed-Metal Oxides of  $\text{NiO}$ ,  $\text{Fe}_2\text{O}_3$ , and  $\text{Mn}_3\text{O}_4$ , *Int. J. Greenhouse Gas Control*, 2008, **2**(1), 21–36, DOI: [10.1016/S1750-5836\(07\)00107-7](https://doi.org/10.1016/S1750-5836(07)00107-7).

92 F. He, X. Li, K. Zhao, Z. Huang, G. Wei and H. Li, The Use of  $\text{La}_{1-x}\text{Sr}_x\text{FeO}_3$  Perovskite-Type Oxides as Oxygen Carriers in Chemical-Looping Reforming of Methane, *Fuel*, 2013, **108**, 465–473, DOI: [10.1016/j.fuel.2012.11.035](https://doi.org/10.1016/j.fuel.2012.11.035).

93 K. Zhao, F. He, Z. Huang, G. Wei, A. Zheng, H. Li and Z. Zhao, Perovskite-Type Oxides  $\text{LaFe}_{1-x}\text{Co}_x\text{O}_3$  for Chemical Looping Steam Methane Reforming to Syngas and Hydrogen Co-Production, *Appl. Energy*, 2016, **168**, 193–203, DOI: [10.1016/j.apenergy.2016.01.052](https://doi.org/10.1016/j.apenergy.2016.01.052).

94 E. Ksepko, Perovskite  $\text{Sr}(\text{Fe}_{1-x}\text{Cu}_x)\text{O}_{3-\delta}$  Materials for Chemical Looping Combustion Applications, *Int. J. Hydrogen Energy*, 2018, **43**(20), 9622–9634, DOI: [10.1016/j.ijhydene.2018.04.046](https://doi.org/10.1016/j.ijhydene.2018.04.046).

95 H.-C. Wu and Y. Ku, Enhanced Performance of Chemical Looping Combustion of Methane with  $\text{Fe}_2\text{O}_3/\text{Al}_2\text{O}_3/\text{TiO}_2$  Oxygen Carrier, *RSC Adv.*, 2018, **8**(70), 39902–39912, DOI: [10.1039/C8RA07863G](https://doi.org/10.1039/C8RA07863G).

96 T. Xu, X. Wang, H. Zhao, B. Xiao, D. Liu and W. Liu, Modulating Lattice Oxygen Activity of  $\text{Ca}_2\text{Fe}_2\text{O}_5$  Brownmillerite for the Co-Production of Syngas and High Purity Hydrogen via Chemical Looping Steam Reforming of Toluene, *Appl. Catal., B*, 2023, **320**, 122010, DOI: [10.1016/j.apcatb.2022.122010](https://doi.org/10.1016/j.apcatb.2022.122010).

97 Y. Cai, C. Wang, M. Zhong, Z. Zhang, B. Xiao, T. Xu and X. Wang, Evaluation of Redox Activity of Brownmillerite-Structured  $\text{Ca}_2\text{Fe}_2\text{O}_5$  Oxygen Carrier for Chemical Looping Applications, *Int. J. Hydrogen Energy*, 2023, **48**(70), 27112–27126, DOI: [10.1016/j.ijhydene.2023.03.395](https://doi.org/10.1016/j.ijhydene.2023.03.395).

98 R. K. Joshi, P. Mohapatra, I. K. Kudva, S. G. Shinde, L. Isom, L. Kovach, J. Pawlikowski, Z. Cheng and L.-S. Fan, Biogas Conversion to Liquid Fuels via Chemical Looping Single Reactor System with  $\text{CO}_2$  Utilization, *Discover Chem. Eng.*, 2023, **3**(1), 13, DOI: [10.1007/s43938-023-00029-2](https://doi.org/10.1007/s43938-023-00029-2).

99 A. Lyngfelt, A. Brink, Ø. Langørgen, T. Mattisson, M. Rydén and C. Linderholm, 11,000 h of Chemical-Looping Combustion Operation—Where Are We and Where Do We Want to Go?, *Int. J. Greenhouse Gas Control*, 2019, **88**, 38–56, DOI: [10.1016/j.ijgpc.2019.05.023](https://doi.org/10.1016/j.ijgpc.2019.05.023).

100 H. Gu, L. Shen, J. Xiao, S. Zhang and T. Song, Chemical Looping Combustion of Biomass/Coal with Natural Iron Ore as Oxygen Carrier in a Continuous Reactor, *Energy Fuels*, 2011, **25**(1), 446–455, DOI: [10.1021/ef101318b](https://doi.org/10.1021/ef101318b).

101 T. Song, J. Wu, H. Zhang and L. Shen, Characterization of an Australia Hematite Oxygen Carrier in Chemical Looping Combustion with Coal, *Int. J. Greenhouse Gas Control*, 2012, **11**, 326–336, DOI: [10.1016/j.ijgpc.2012.08.013](https://doi.org/10.1016/j.ijgpc.2012.08.013).



102 S. Jiang, L. Shen, J. Yan, H. Ge and H. Gu, Performance in Chemical Looping Staged Combustion of Coal by Using Hematite as Oxygen Carrier, *Ind. Eng. Chem. Res.*, 2018, 57(48), 16486–16494, DOI: [10.1021/acs.iecr.8b03788](https://doi.org/10.1021/acs.iecr.8b03788).

103 S. Jiang, L. Shen, J. Yan, H. Ge and T. Song, Performance in Coupled Fluidized Beds for Chemical Looping Combustion of CO and Biomass Using Hematite as an Oxygen Carrier, *Energy Fuels*, 2018, 32(12), 12721–12729, DOI: [10.1021/acs.energyfuels.8b02861](https://doi.org/10.1021/acs.energyfuels.8b02861).

104 A. Evdou, V. Zaspalis and L. Nalbandian, Ferrites as Redox Catalysts for Chemical Looping Processes, *Fuel*, 2016, 165, 367–378, DOI: [10.1016/j.fuel.2015.10.049](https://doi.org/10.1016/j.fuel.2015.10.049).

105 G. Wei, F. He, Z. Huang, A. Zheng, K. Zhao and H. Li, Continuous Operation of a 10 kW<sub>th</sub> Chemical Looping Integrated Fluidized Bed Reactor for Gasifying Biomass Using an Iron-Based Oxygen Carrier, *Energy Fuels*, 2015, 29(1), 233–241, DOI: [10.1021/ef5021457](https://doi.org/10.1021/ef5021457).

106 G. Wei, F. He, Z. Zhao, Z. Huang, A. Zheng, K. Zhao and H. Li, Performance of Fe–Ni Bimetallic Oxygen Carriers for Chemical Looping Gasification of Biomass in a 10 kW<sub>th</sub> Interconnected Circulating Fluidized Bed Reactor, *Int. J. Hydrogen Energy*, 2015, 40(46), 16021–16032, DOI: [10.1016/j.ijhydene.2015.09.128](https://doi.org/10.1016/j.ijhydene.2015.09.128).

107 S. Wang, G. Wang, F. Jiang, M. Luo and H. Li, Chemical Looping Combustion of Coke Oven Gas by Using Fe<sub>2</sub>O<sub>3</sub>/CuO with MgAl<sub>2</sub>O<sub>4</sub> as Oxygen Carrier, *Energy Environ. Sci.*, 2010, 3(9), 1353, DOI: [10.1039/b926193a](https://doi.org/10.1039/b926193a).

108 R. Siriwardane, J. Riley, S. Bayham, D. Straub, H. Tian, J. Weber and G. Richards, 50-kW<sub>th</sub> Methane/Air Chemical Looping Combustion Tests with Commercially Prepared CuO–Fe<sub>2</sub>O<sub>3</sub>–Alumina Oxygen Carrier with Two Different Techniques, *Appl. Energy*, 2018, 213, 92–99, DOI: [10.1016/j.apenergy.2018.01.016](https://doi.org/10.1016/j.apenergy.2018.01.016).

109 S. Bayham, D. Straub and J. Weber, Operation of a 50-kW<sub>th</sub> Chemical Looping Combustion Test Facility under Autothermal Conditions, *Int. J. Greenhouse Gas Control*, 2019, 87, 211–220, DOI: [10.1016/j.ijggc.2019.05.022](https://doi.org/10.1016/j.ijggc.2019.05.022).

110 N. Berguerand and A. Lyngfelt, Design and Operation of a 10 kW<sub>th</sub> Chemical-Looping Combustor for Solid Fuels – Testing with South African Coal, *Fuel*, 2008, 87(12), 2713–2726, DOI: [10.1016/j.fuel.2008.03.008](https://doi.org/10.1016/j.fuel.2008.03.008).

111 N. Berguerand and A. Lyngfelt, The Use of Petroleum Coke as Fuel in a 10 kW<sub>th</sub> Chemical-Looping Combustor, *Int. J. Greenhouse Gas Control*, 2008, 2(2), 169–179, DOI: [10.1016/j.ijgge.2007.12.004](https://doi.org/10.1016/j.ijgge.2007.12.004).

112 N. Berguerand and A. Lyngfelt, Chemical-Looping Combustion of Petroleum Coke Using Ilmenite in a 10 kW<sub>th</sub> Unit–High-Temperature Operation, *Energy Fuels*, 2009, 23(10), 5257–5268, DOI: [10.1021/ef900464j](https://doi.org/10.1021/ef900464j).

113 N. Berguerand and A. Lyngfelt, Operation in a 10 kW<sub>th</sub> Chemical-Looping Combustor for Solid Fuel–Testing with a Mexican Petroleum Coke, *Energy Procedia*, 2009, 1(1), 407–414, DOI: [10.1016/j.egypro.2009.01.055](https://doi.org/10.1016/j.egypro.2009.01.055).

114 P. Markström, C. Linderholm and A. Lyngfelt, Chemical-Looping Combustion of Solid Fuels – Design and Operation of a 100 kW Unit with Bituminous Coal, *Int. J. Greenhouse Gas Control*, 2013, 15, 150–162, DOI: [10.1016/j.ijggc.2013.01.048](https://doi.org/10.1016/j.ijggc.2013.01.048).

115 P. Markström, C. Linderholm and A. Lyngfelt, Analytical Model of Gas Conversion in a 100 kW Chemical-Looping Combustor for Solid Fuels—Comparison with Operational Results, *Chem. Eng. Sci.*, 2013, 96, 131–141, DOI: [10.1016/j.ces.2013.04.001](https://doi.org/10.1016/j.ces.2013.04.001).

116 J. Ma, H. Zhao, X. Tian, Y. Wei, S. Rajendran, Y. Zhang, S. Bhattacharya and C. Zheng, Chemical Looping Combustion of Coal in a 5 kW<sub>th</sub> Interconnected Fluidized Bed Reactor Using Hematite as Oxygen Carrier, *Appl. Energy*, 2015, 157, 304–313, DOI: [10.1016/j.apenergy.2015.03.124](https://doi.org/10.1016/j.apenergy.2015.03.124).

117 H. Ge, W. Guo, L. Shen, T. Song and J. Xiao, Biomass Gasification Using Chemical Looping in a 25 kW<sub>th</sub> Reactor with Natural Hematite as Oxygen Carrier, *Chem. Eng. J.*, 2016, 286, 174–183, DOI: [10.1016/j.cej.2015.10.092](https://doi.org/10.1016/j.cej.2015.10.092).

118 P. Ohlemüller, J.-P. Busch, M. Reitz, J. Ströhle and B. Epple, Chemical-Looping Combustion of Hard Coal: Autothermal Operation of a 1 MW<sub>th</sub> Pilot Plant, *J. Energy Resour. Technol.*, 2016, 138(4), 042203, DOI: [10.1115/1.4032357](https://doi.org/10.1115/1.4032357).

119 P. Ohlemüller, J. Ströhle and B. Epple, Chemical Looping Combustion of Hard Coal and Torrefied Biomass in a 1 MW<sub>th</sub> Pilot Plant, *Int. J. Greenhouse Gas Control*, 2017, 65, 149–159, DOI: [10.1016/j.ijggc.2017.08.013](https://doi.org/10.1016/j.ijggc.2017.08.013).

120 J. Ströhle, M. Orth and B. Epple, Chemical Looping Combustion of Hard Coal in a 1 MW<sub>th</sub> Pilot Plant Using Ilmenite as Oxygen Carrier, *Appl. Energy*, 2015, 157, 288–294, DOI: [10.1016/j.apenergy.2015.06.035](https://doi.org/10.1016/j.apenergy.2015.06.035).

121 S. C. Bayham, H. R. Kim, D. Wang, A. Tong, L. Zeng, O. McGiveron, M. V. Kathe, E. Chung, W. Wang, A. Wang, A. Majumder and L.-S. Fan, Iron-Based Coal Direct Chemical Looping Combustion Process: 200-h Continuous Operation of a 25-kW<sub>th</sub> Subpilot Unit, *Energy Fuels*, 2013, 27(3), 1347–1356, DOI: [10.1021/ef400010s](https://doi.org/10.1021/ef400010s).

122 L. Shen, J. Wu, J. Xiao, Q. Song and R. Xiao, Chemical-Looping Combustion of Biomass in a 10 kW<sub>th</sub> Reactor with Iron Oxide As an Oxygen Carrier, *Energy Fuels*, 2009, 23(5), 2498–2505, DOI: [10.1021/ef900033n](https://doi.org/10.1021/ef900033n).

123 S. R. Son and S. D. Kim, Chemical-Looping Combustion with NiO and Fe<sub>2</sub>O<sub>3</sub> in a Thermobalance and Circulating Fluidized Bed Reactor with Double Loops, *Ind. Eng. Chem. Res.*, 2006, 45(8), 2689–2696, DOI: [10.1021/ie050919x](https://doi.org/10.1021/ie050919x).

124 S. Bayham, D. Straub and J. Weber, *Operation of the NETL Chemical Looping Reactor with Natural Gas and a Novel Copper-Iron Material*, NETL-PUB-20912, 1347568, 2017, DOI: [10.2172/1347568](https://doi.org/10.2172/1347568).

125 C. Linderholm and M. Schmitz, Chemical-Looping Combustion of Solid Fuels in a 100 kW Dual Circulating Fluidized Bed System Using Iron Ore as Oxygen Carrier, *J. Environ. Chem. Eng.*, 2016, 4(1), 1029–1039, DOI: [10.1016/j.jecee.2016.01.006](https://doi.org/10.1016/j.jecee.2016.01.006).

126 C. Linderholm, M. Schmitz, P. Knutsson, M. Källén and A. Lyngfelt, Use of Low-Volatile Solid Fuels in a 100 kW Chemical-Looping Combustor, *Energy Fuels*, 2014, 28(9), 5942–5952, DOI: [10.1021/ef501067b](https://doi.org/10.1021/ef501067b).



127 A. Corcoran, J. Marinkovic, F. Lind, H. Thunman, P. Knutsson and M. Seemann, Ash Properties of Ilmenite Used as Bed Material for Combustion of Biomass in a Circulating Fluidized Bed Boiler, *Energy Fuels*, 2014, **28**(12), 7672–7679, DOI: [10.1021/ef501810u](https://doi.org/10.1021/ef501810u).

128 R. Pérez-Vega, A. Abad, F. García-Labiano, P. Gayán, L. F. de Diego and J. Adámez, Coal Combustion in a 50 kW<sub>th</sub> Chemical Looping Combustion Unit: Seeking Operating Conditions to Maximize CO<sub>2</sub> Capture and Combustion Efficiency, *Int. J. Greenhouse Gas Control*, 2016, **50**, 80–92, DOI: [10.1016/j.ijgge.2016.04.006](https://doi.org/10.1016/j.ijgge.2016.04.006).

129 P. Kolbitsch, J. Bolhàr-Nordenkampf, T. Pröll and H. Hofbauer, Operating Experience with Chemical Looping Combustion in a 120 kW Dual Circulating Fluidized Bed (DCFB) Unit, *Int. J. Greenhouse Gas Control*, 2010, **4**(2), 180–185, DOI: [10.1016/j.ijgge.2009.09.014](https://doi.org/10.1016/j.ijgge.2009.09.014).

130 C. Linderholm, M. Schmitz, P. Knutsson and A. Lyngfelt, Chemical-Looping Combustion in a 100-kW Unit Using a Mixture of Ilmenite and Manganese Ore as Oxygen Carrier, *Fuel*, 2016, **166**, 533–542, DOI: [10.1016/j.fuel.2015.11.015](https://doi.org/10.1016/j.fuel.2015.11.015).

131 J. Bao, L. Chen, F. Liu, Z. Fan, H. S. Nikolic and K. Liu, Evaluating the Effect of Inert Supports and Alkali Sodium on the Performance of Red Mud Oxygen Carrier in Chemical Looping Combustion, *Ind. Eng. Chem. Res.*, 2016, **55**(29), 8046–8057, DOI: [10.1021/acs.iecr.6b01835](https://doi.org/10.1021/acs.iecr.6b01835).

132 M. M. Tijani, A. Aqsha and N. Mahinpey, Synthesis and study of metal-based oxygen carriers (Cu, Co, Fe, Ni) and their interaction with supported metal oxides (Al<sub>2</sub>O<sub>3</sub>, CeO<sub>2</sub>, TiO<sub>2</sub>, ZrO<sub>2</sub>) in a chemical looping combustion system, *Energy*, 2017, **138**, 873–882, DOI: [10.1016/j.energy.2017.07.100](https://doi.org/10.1016/j.energy.2017.07.100).

133 N. C. Means, S. Hammache, W. A. Burgess, B. H. Howard and M. W. Smith, Evaluation of the Redox Performance and Characterization of Fe<sub>2</sub>O<sub>3</sub>/CeO<sub>2</sub>/ZrO<sub>2</sub> Oxygen Carriers under High Temperature in Situ Gasification Chemical-Looping Combustion Conditions, *Energy Fuels*, 2020, **34**(1), 871–878, DOI: [10.1021/acs.energyfuels.9b03018](https://doi.org/10.1021/acs.energyfuels.9b03018).

134 Y. Liu, L. Qin, Z. Cheng, J. W. Goetze, F. Kong, J. A. Fan and L.-S. Fan, Near 100% CO Selectivity in Nanoscaled Iron-Based Oxygen Carriers for Chemical Looping Methane Partial Oxidation, *Nat. Commun.*, 2019, **10**(1), 5503, DOI: [10.1038/s41467-019-13560-0](https://doi.org/10.1038/s41467-019-13560-0).

135 S. Hu, Q. Chen, J. Xiang, S. Su, L. Sun, Y. Wang, B. Xu and H. Chi, Modification of Iron Oxide to Promote Reaction Property for Chemical Looping Combustion with CO, *Combust. Sci. Technol.*, 2016, **188**(8), 1319–1330, DOI: [10.1080/00102202.2016.1190345](https://doi.org/10.1080/00102202.2016.1190345).

136 X. Chen, S. Zhang, R. Xiao and P. Li, Modification of Traditionally Impregnated Fe<sub>2</sub>O<sub>3</sub>/Al<sub>2</sub>O<sub>3</sub> Oxygen Carriers by Ultrasonic Method and Their Performance in Chemical Looping Combustion, *Greenhouse Gases: Sci. Technol.*, 2017, **7**(1), 65–77, DOI: [10.1002/ghg.1636](https://doi.org/10.1002/ghg.1636).

137 L. Liu and M. R. Zachariah, Enhanced Performance of Alkali Metal Doped Fe<sub>2</sub>O<sub>3</sub> and Fe<sub>2</sub>O<sub>3</sub>/Al<sub>2</sub>O<sub>3</sub> Composites As Oxygen Carrier Material in Chemical Looping Combustion, *Energy Fuels*, 2013, **27**(8), 4977–4983, DOI: [10.1021/ef400748x](https://doi.org/10.1021/ef400748x).

138 W.-C. Huang, Y.-L. Kuo, Y.-M. Su, Y.-H. Tseng, H.-Y. Lee and Y. Ku, A Facile Method for Sodium-Modified Fe<sub>2</sub>O<sub>3</sub>/Al<sub>2</sub>O<sub>3</sub> Oxygen Carrier by an Air Atmospheric Pressure Plasma Jet for Chemical Looping Combustion Process, *Chem. Eng. J.*, 2017, **316**, 15–23, DOI: [10.1016/j.cej.2017.01.078](https://doi.org/10.1016/j.cej.2017.01.078).

139 L. Qin, M. Guo, Z. Cheng, M. Xu, Y. Liu, D. Xu, J. A. Fan and L.-S. Fan, Improved Cyclic Redox Reactivity of Lanthanum Modified Iron-Based Oxygen Carriers in Carbon Monoxide Chemical Looping Combustion, *J. Mater. Chem. A*, 2017, **5**(38), 20153–20160, DOI: [10.1039/C7TA04228K](https://doi.org/10.1039/C7TA04228K).

140 S. Bhavsar, N. Isenberg, A. More and G. Veser, Lanthana-Doped Ceria as Active Support for Oxygen Carriers in Chemical Looping Combustion, *Appl. Energy*, 2016, **168**, 236–247, DOI: [10.1016/j.apenergy.2016.01.073](https://doi.org/10.1016/j.apenergy.2016.01.073).

141 J. He, Q. Yang, Z. Song, W. Chang, C. Huang, Y. Zhu, X. Ma and X. Wang, Improving the Carbon Resistance of Iron-Based Oxygen Carrier for Hydrogen Production via Chemical Looping Steam Methane Reforming: A Review, *Fuel*, 2023, **351**, 128864, DOI: [10.1016/j.fuel.2023.128864](https://doi.org/10.1016/j.fuel.2023.128864).

142 X. Yin, S. Wang, B. Wang and L. Shen, Perovskite-Type LaMn<sub>1-x</sub>B<sub>x</sub>O<sub>3+δ</sub> (B = Fe, Co and Ni) as Oxygen Carriers for Chemical Looping Steam Methane Reforming, *Chem. Eng. J.*, 2021, **422**, 128751, DOI: [10.1016/j.cej.2021.128751](https://doi.org/10.1016/j.cej.2021.128751).

143 C. Lin, W. Qin and C. Dong, Reduction Effect of α-Fe<sub>2</sub>O<sub>3</sub> on Carbon Deposition and CO Oxidation during Chemical-Looping Combustion, *Chem. Eng. J.*, 2016, **301**, 257–265, DOI: [10.1016/j.cej.2016.04.136](https://doi.org/10.1016/j.cej.2016.04.136).

144 Q. Yang, L. Chen, N. Jin, Y. Zhu, J. He, P. Zhao, C. Huang, L. Wei, X. Ma and X. Wang, Boosted Carbon Resistance of Ceria-Hexaaluminate by in-Situ Formed CeFe<sub>x</sub>Al<sub>1-x</sub>O<sub>3</sub> as Oxygen Pool for Chemical Looping Dry Reforming of Methane, *Appl. Catal., B*, 2023, **330**, 122636, DOI: [10.1016/j.apcatb.2023.122636](https://doi.org/10.1016/j.apcatb.2023.122636).

145 D. D. Miller, R. Siriwardane and J. Poston, Fluidized-Bed and Fixed-Bed Reactor Testing of Methane Chemical Looping Combustion with MgO-Promoted Hematite, *Appl. Energy*, 2015, **146**, 111–121, DOI: [10.1016/j.apenergy.2015.02.047](https://doi.org/10.1016/j.apenergy.2015.02.047).

146 W. Liu, L. Shen, H. Gu and L. Wu, Chemical Looping Hydrogen Generation Using Potassium-Modified Iron Ore as an Oxygen Carrier, *Energy Fuels*, 2016, **30**(3), 1756–1763, DOI: [10.1021/acs.energyfuels.5b02280](https://doi.org/10.1021/acs.energyfuels.5b02280).

147 L. Wang, L. Shen, W. Liu and S. Jiang, Chemical Looping Hydrogen Generation Using Synthesized Hematite-Based Oxygen Carrier Comodified by Potassium and Copper, *Energy Fuels*, 2017, **31**(8), 8423–8433, DOI: [10.1021/acs.energyfuels.7b01190](https://doi.org/10.1021/acs.energyfuels.7b01190).

148 L. Wang, L. Shen, S. Jiang and W. Liu, Inhibition of Carbon Deposition Using Iron Ore Modified by K and Cu in Chemical Looping Hydrogen Generation, *Int. J. Energy Res.*, 2019, **43**(1), 167–180, DOI: [10.1002/er.4246](https://doi.org/10.1002/er.4246).

149 X. Cheng, Z. Gu, F. Li, X. Zhu, Y. Wei, M. Zheng, D. Tian, H. Wang and K. Li, Enhanced Resistance to Carbon Deposition in Chemical-Looping Combustion of Methane:



Synergistic Effect of Different Oxygen Carriers via Sequence Filling, *Chem. Eng. J.*, 2021, **421**, 129776, DOI: [10.1016/j.cej.2021.129776](https://doi.org/10.1016/j.cej.2021.129776).

150 Y. Liu, K. Yin, J. Wu, D. Mei, J. Konttinen, T. Joronen, Z. Hu and C. He, Ash Chemistry in Chemical Looping Process for Biomass Valorization: A Review, *Chem. Eng. J.*, 2023, **478**, 147429, DOI: [10.1016/j.cej.2023.147429](https://doi.org/10.1016/j.cej.2023.147429).

151 Z. Miao, L. Shen, Z. Li and T. Shen, Sintering and Agglomeration Characteristics of Industrially Prepared  $\text{CaMn}_{0.5}\text{Ti}_{0.375}\text{Fe}_{0.125}\text{O}_{3-\delta}$  Perovskite Oxygen Carrier in Chemical Looping Combustion, *Chem. Eng. J.*, 2023, **472**, 144722, DOI: [10.1016/j.cej.2023.144722](https://doi.org/10.1016/j.cej.2023.144722).

152 S. C. Bayham, R. Breault and E. Monazam, Particulate Solid Attrition in CFB Systems – An Assessment for Emerging Technologies, *Powder Technol.*, 2016, **302**, 42–62, DOI: [10.1016/j.powtec.2016.08.016](https://doi.org/10.1016/j.powtec.2016.08.016).

153 F. Liu, C. Song, D. Zhu, C. Li, L. Ai, C. Xin, X. Zeng, L. Zeng, N. Huang and L. Yang, Attrition and Attrition-Resistance of Oxygen Carrier in Chemical Looping Process – A Comprehensive Review, *Fuel*, 2023, **333**, 126304, DOI: [10.1016/j.fuel.2022.126304](https://doi.org/10.1016/j.fuel.2022.126304).

154 Y. De Vos, M. Jacobs, P. Van Der Voort, I. Van Driessche, F. Snijkers and A. Verberckmoes, Sustainable Iron-Based Oxygen Carriers for Chemical Looping for Hydrogen Generation, *Int. J. Hydrogen Energy*, 2019, **44**(3), 1374–1391, DOI: [10.1016/j.ijhydene.2018.11.099](https://doi.org/10.1016/j.ijhydene.2018.11.099).

155 Y. Ku, H.-C. Wu, P.-C. Chiu, Y.-H. Tseng and Y.-L. Kuo, Methane Combustion by Moving Bed Fuel Reactor with  $\text{Fe}_2\text{O}_3/\text{Al}_2\text{O}_3$  Oxygen Carriers, *Appl. Energy*, 2014, **113**, 1909–1915, DOI: [10.1016/j.apenergy.2013.06.014](https://doi.org/10.1016/j.apenergy.2013.06.014).

156 Y. Kang, M. Tian, C. Huang, J. Lin, B. Hou, X. Pan, L. Li, A. I. Rykov, J. Wang and X. Wang, Improving Syngas Selectivity of  $\text{Fe}_2\text{O}_3/\text{Al}_2\text{O}_3$  with Yttrium Modification in Chemical Looping Methane Conversion, *ACS Catal.*, 2019, **9**(9), 8373–8382, DOI: [10.1021/acscatal.9b02730](https://doi.org/10.1021/acscatal.9b02730).

157 Y. Kang, Y. Han, M. Tian, C. Huang, C. Wang, J. Lin, B. Hou, Y. Su, L. Li, J. Wang and X. Wang, Promoted Methane Conversion to Syngas over Fe-Based Garnets via Chemical Looping, *Appl. Catal., B*, 2020, **278**, 119305, DOI: [10.1016/j.apcatb.2020.119305](https://doi.org/10.1016/j.apcatb.2020.119305).

158 I. H. Son, S. Kwon, J. H. Park and S. J. Lee, High Coke-Resistance  $\text{MgAl}_2\text{O}_4$  Islands Decorated Catalyst with Minimizing Sintering in Carbon Dioxide Reforming of Methane, *Nano Energy*, 2016, **19**, 58–67, DOI: [10.1016/j.nanoen.2015.11.007](https://doi.org/10.1016/j.nanoen.2015.11.007).

159 F. Liu, L. Chen, J. K. Neathery, K. Saito and K. Liu, Cerium Oxide Promoted Iron-Based Oxygen Carrier for Chemical Looping Combustion, *Ind. Eng. Chem. Res.*, 2014, **53**(42), 16341–16348, DOI: [10.1021/ie503160b](https://doi.org/10.1021/ie503160b).

160 S. Ma, S. Chen, Z. Zhao, A. Soomro, M. Zhu, J. Hu, M. Wu and W. Xiang, Enhanced Hydrogen Generation for  $\text{Fe}_2\text{O}_3/\text{CeO}_2$  Oxygen Carrier via Rare-Earth (Y, Sm, and La) Doping in Chemical Looping Process, *Energy Fuels*, 2018, **32**(11), 11362–11374, DOI: [10.1021/acs.energyfuels.8b02758](https://doi.org/10.1021/acs.energyfuels.8b02758).

161 R. Schmitt, A. Nenning, O. Kraynis, R. Korobko, A. I. Frenkel, I. Lubomirsky, S. M. Haile and J. L. M. Rupp, A Review of Defect Structure and Chemistry in Ceria and Its Solid Solutions, *Chem. Soc. Rev.*, 2020, **49**(2), 554–592, DOI: [10.1039/C9CS00588A](https://doi.org/10.1039/C9CS00588A).

162 J. Y. Do, N. Son, N.-K. Park, B. S. Kwak, J.-I. Baek, H.-J. Ryu and M. Kang, Reliable Oxygen Transfer in  $\text{MgAl}_2\text{O}_4$  Spinel through the Reversible Formation of Oxygen Vacancies by  $\text{Cu}^{2+}/\text{Fe}^{3+}$  Anchoring, *Appl. Energy*, 2018, **219**, 138–150, DOI: [10.1016/j.apenergy.2018.03.041](https://doi.org/10.1016/j.apenergy.2018.03.041).

163 S. Zhang, Y. Feng and X. Guo, Redox Performance of Cu-Doped  $\text{Fe}_2\text{O}_3/\text{Al}_2\text{O}_3$  as Oxygen Carriers for Chemical Looping Hydrogen Production, *Energy Fuels*, 2021, **35**(1), 626–635, DOI: [10.1021/acs.energyfuels.0c03496](https://doi.org/10.1021/acs.energyfuels.0c03496).

164 K.-S. Kang, C.-H. Kim, W.-C. Cho, K.-K. Bae, S.-W. Woo and C.-S. Park, Reduction Characteristics of  $\text{CuFe}_2\text{O}_4$  and  $\text{Fe}_3\text{O}_4$  by Methane;  $\text{CuFe}_2\text{O}_4$  as an Oxidant for Two-Step Thermochemical Methane Reforming, *Int. J. Hydrogen Energy*, 2008, **33**(17), 4560–4568, DOI: [10.1016/j.ijhydene.2008.05.054](https://doi.org/10.1016/j.ijhydene.2008.05.054).

165 J. Chen, K. Zhao, Z. Zhao, F. He, Z. Huang and G. Wei, Identifying the Roles of  $\text{MFe}_2\text{O}_4$  ( $\text{M}=\text{Cu, Ba, Ni, and Co}$ ) in the Chemical Looping Reforming of Char, Pyrolysis Gas and Tar Resulting from Biomass Pyrolysis, *Int. J. Hydrogen Energy*, 2019, **44**(10), 4674–4687, DOI: [10.1016/j.ijhydene.2018.12.216](https://doi.org/10.1016/j.ijhydene.2018.12.216).

166 Z. Ma, S. Zhang, R. Xiao and J. Wang, Inhibited Phase Segregation to Enhance the Redox Performance of  $\text{NiFe}_2\text{O}_4$  via  $\text{CeO}_2$  Modification in the Chemical Looping Process, *Energy Fuels*, 2020, **34**(5), 6178–6185, DOI: [10.1021/acs.energyfuels.0c00686](https://doi.org/10.1021/acs.energyfuels.0c00686).

167 Z. Huang, N. Gao, Y. Lin, G. Wei, K. Zhao, A. Zheng, Z. Zhao, H. Yuan and H. Li, Exploring the Migration and Transformation of Lattice Oxygen during Chemical Looping with  $\text{NiFe}_2\text{O}_4$  Oxygen Carrier, *Chem. Eng. J.*, 2022, **429**, 132064, DOI: [10.1016/j.cej.2021.132064](https://doi.org/10.1016/j.cej.2021.132064).

168 J. Gao, G. Pu, S. Jia, C. Yuan and C. Zhang, Study on the Redox Performance of Cu and Ce-doped  $\text{CoFe}_2\text{O}_4$  as Oxygen Carriers for Chemical Looping Hydrogen Generation, *Int. J. Energy Res.*, 2022, **46**(6), 7424–7440, DOI: [10.1002/er.7650](https://doi.org/10.1002/er.7650).

169 X. Zhang, C. Pei, X. Chang, S. Chen, R. Liu, Z.-J. Zhao, R. Mu and J. Gong,  $\text{FeO}_6$  Octahedral Distortion Activates Lattice Oxygen in Perovskite Ferrite for Methane Partial Oxidation Coupled with  $\text{CO}_2$  Splitting, *J. Am. Chem. Soc.*, 2020, **142**(26), 11540–11549, DOI: [10.1021/jacs.0c04643](https://doi.org/10.1021/jacs.0c04643).

170 F. Huang, M. Tian, Y. Zhu, X. Wang, A. Wang, L. Li, J. Lin and J. Wang, Fe-Substituted Ba-Hexaaluminate with Enhanced Oxygen Mobility for  $\text{CO}_2$  Capture by Chemical Looping Combustion of Methane, *J. Energy Chem.*, 2019, **29**, 50–57, DOI: [10.1016/j.jechem.2018.02.003](https://doi.org/10.1016/j.jechem.2018.02.003).

171 Y. Zhu, W. Liu, X. Sun, X. Ma, Y. Kang, X. Wang and J. Wang, La-hexaaluminate for Synthesis Gas Generation by Chemical Looping Partial Oxidation of Methane Using  $\text{CO}_2$  as Sole Oxidant, *AIChE J.*, 2018, **64**(2), 550–563, DOI: [10.1002/aic.15942](https://doi.org/10.1002/aic.15942).

172 Y. Wang, X. Tian, H. Zhao and K. Liu, The Use of a Low-Cost Oxygen Carrier Prepared from Red Mud and Copper Ore for in Situ Gasification Chemical Looping Combustion of Coal,



*Fuel Process. Technol.*, 2020, **205**, 106460, DOI: [10.1016/j.fuproc.2020.106460](https://doi.org/10.1016/j.fuproc.2020.106460).

173 M. M. Azis, H. Leion, E. Jerndal, B. -M. Steenari, T. Mattisson and A. Lyngfelt, The Effect of Bituminous and Lignite Ash on the Performance of Ilmenite as Oxygen Carrier in Chemical-Looping Combustion, *Chem. Eng. Technol.*, 2013, **36**(9), 1460–1468, DOI: [10.1002/ceat.201200608](https://doi.org/10.1002/ceat.201200608).

174 S. V. Vassilev, D. Baxter and C. G. Vassileva, An Overview of the Behaviour of Biomass during Combustion: Part I. Phase-Mineral Transformations of Organic and Inorganic Matter, *Fuel*, 2013, **112**, 391–449, DOI: [10.1016/j.fuel.2013.05.043](https://doi.org/10.1016/j.fuel.2013.05.043).

175 K. Yin, H. Wang, A. Veksha, X. Dou, D. Khairunnisa Binte Mohamed, S. Heberlein, G. Liu, W. Chen and G. Lisak, Oxygen Carriers from Incineration Bottom Ash for Chemical Looping Combustion of Syngas: Effect of Composition on Combustion Efficiency, *Chem. Eng. J.*, 2021, **405**, 127068, DOI: [10.1016/j.cej.2020.127068](https://doi.org/10.1016/j.cej.2020.127068).

176 L. Mu, T. Li, Z. Wang, Y. Shang and H. Yin, Influence of Water/Acid Washing Pretreatment of Aquatic Biomass on Ash Transformation and Slagging Behavior during Co-Firing with Bituminous Coal, *Energy*, 2021, **234**, 121286, DOI: [10.1016/j.energy.2021.121286](https://doi.org/10.1016/j.energy.2021.121286).

177 D. Mazerolle, H. Rezaei, B. Bronson, L. Nguyen and F. Preto, Sieving and Acid Washing as a Pretreatment to Fast Pyrolysis of a High Ash Hog Fuel, *Energy Fuels*, 2019, **33**(6), 5352–5359, DOI: [10.1021/acs.energyfuels.9b00694](https://doi.org/10.1021/acs.energyfuels.9b00694).

178 B. Wang, R. Yan, H. Zhao, Y. Zheng, Z. Liu and C. Zheng, Investigation of Chemical Looping Combustion of Coal with  $\text{CuFe}_2\text{O}_4$  Oxygen Carrier, *Energy Fuels*, 2011, **25**(7), 3344–3354, DOI: [10.1021/ef2004078](https://doi.org/10.1021/ef2004078).

179 S. Liu, F. He, Z. Huang, A. Zheng, Y. Feng, Y. Shen, H. li, H. Wu and P. Glarborg, Screening of  $\text{NiFe}_2\text{O}_4$  Nanoparticles as Oxygen Carrier in Chemical Looping Hydrogen Production, *Energy Fuels*, 2016, **30**(5), 4251–4262, DOI: [10.1021/acs.energyfuels.6b00284](https://doi.org/10.1021/acs.energyfuels.6b00284).

180 G. Liu, Y. Liao, Y. Wu and X. Ma, Reactivity of Co-Doped  $\text{Ca}_2\text{Fe}_2\text{O}_5$  Brownmillerite Oxides as Oxygen Carriers for Microalgae Chemical Looping Gasification, *Int. J. Hydrogen Energy*, 2019, **44**(5), 2546–2559, DOI: [10.1016/j.ijhydene.2018.11.232](https://doi.org/10.1016/j.ijhydene.2018.11.232).

181 B. Purnama and A. T. Wijayanta, Suharyana. Effect of Calcination Temperature on Structural and Magnetic Properties in Cobalt Ferrite Nano Particles, *J. King Saud Univ., Sci.*, 2019, **31**(4), 956–960, DOI: [10.1016/j.jksus.2018.07.019](https://doi.org/10.1016/j.jksus.2018.07.019).

182 A. Irhamsyah, L. Lusiana, S. Wannapaiboon, Ma. Baqiyah and S. Pratapa, Synthesis of Pseudobrookite  $\text{Fe}_{2-x}\text{Al}_x\text{TiO}_5$  ( $0 \leq x \leq 0.5$ ) Powders, *J. Phys.:Conf. Ser.*, 2021, **1951**(1), 012019, DOI: [10.1088/1742-6596/1951/1/012019](https://doi.org/10.1088/1742-6596/1951/1/012019).

183 P. Cho, T. Mattisson and A. Lyngfelt, Defluidization Conditions for a Fluidized Bed of Iron Oxide-, Nickel Oxide-, and Manganese Oxide-Containing Oxygen Carriers for Chemical-Looping Combustion, *Ind. Eng. Chem. Res.*, 2005, **45**(3), 968–977, DOI: [10.1021/ie050484d](https://doi.org/10.1021/ie050484d).

184 J. Ji and L. Shen, Enhanced Morphological Maintenance and Redox Stability by Dispersing Nickel Ferrite into Silica Matrix for Chemical Looping Hydrogen Production via Water Splitting, *Fuel Process. Technol.*, 2023, **251**, 107946, DOI: [10.1016/j.fuproc.2023.107946](https://doi.org/10.1016/j.fuproc.2023.107946).

185 Z. Huang, H. Jiang, F. He, D. Chen, G. Wei, K. Zhao, A. Zheng, Y. Feng, Z. Zhao and H. Li, Evaluation of Multi-Cycle Performance of Chemical Looping Dry Reforming Using  $\text{CO}_2$  as an Oxidant with Fe–Ni Bimetallic Oxides, *J. Energy Chem.*, 2016, **25**(1), 62–70, DOI: [10.1016/j.jecchem.2015.10.008](https://doi.org/10.1016/j.jecchem.2015.10.008).

186 S. M. Olhero, D. Soma, V. S. Amaral, T. W. Button, F. J. Alves and J. M. F. Ferreira, Co-Precipitation of a Ni–Zn Ferrite Precursor Powder: Effects of Heat Treatment Conditions and Deagglomeration on the Structure and Magnetic Properties, *J. Eur. Ceram. Soc.*, 2012, **32**(10), 2469–2476, DOI: [10.1016/j.jeurceramsoc.2012.03.017](https://doi.org/10.1016/j.jeurceramsoc.2012.03.017).

187 A. Mishra and F. Li, Chemical Looping at the Nanoscale—Challenges and Opportunities, *Curr. Opin. Chem. Eng.*, 2018, **20**, 143–150, DOI: [10.1016/j.coche.2018.05.001](https://doi.org/10.1016/j.coche.2018.05.001).

188 *Handbook of Fluidization and Fluid-Particle Systems*, ed. Yang, W.-C., CRC Press, 2003, DOI: [10.1201/9780203912744](https://doi.org/10.1201/9780203912744).

189 A. Cabello, C. Dueso, F. García-Labiano, P. Gayán, A. Abad, L. F. de Diego and J. Adánez, Performance of a Highly Reactive Impregnated  $\text{Fe}_2\text{O}_3/\text{Al}_2\text{O}_3$  Oxygen Carrier with  $\text{CH}_4$  and  $\text{H}_2\text{S}$  in a 500  $\text{W}_{\text{th}}$  CLC Unit, *Fuel*, 2014, **121**, 117–125, DOI: [10.1016/j.fuel.2013.12.027](https://doi.org/10.1016/j.fuel.2013.12.027).

190 M. A. Pans, P. Gayán, L. F. de Diego, F. García-Labiano, A. Abad and J. Adánez, Performance of a Low-Cost Iron Ore as an Oxygen Carrier for Chemical Looping Combustion of Gaseous Fuels, *Chem. Eng. Res. Des.*, 2015, **93**, 736–746, DOI: [10.1016/j.cherd.2014.07.001](https://doi.org/10.1016/j.cherd.2014.07.001).

191 D. Mei, T. Mendiara, A. Abad, L. F. de Diego, F. García-Labiano, P. Gayán, J. Adánez and H. Zhao, Evaluation of Manganese Minerals for Chemical Looping Combustion, *Energy Fuels*, 2015, **29**(10), 6605–6615, DOI: [10.1021/acs.energyfuels.5b01293](https://doi.org/10.1021/acs.energyfuels.5b01293).

192 C. Chung, L. Qin, V. Shah and L.-S. Fan, Chemically and Physically Robust, Commercially-Viable Iron-Based Composite Oxygen Carriers Sustainable over 3000 Redox Cycles at High Temperatures for Chemical Looping Applications, *Energy Environ. Sci.*, 2017, **10**(11), 2318–2323, DOI: [10.1039/C7EE02657A](https://doi.org/10.1039/C7EE02657A).

